~~Towards ground-to-space radiative closure in the~~ Validation of PREFIRE mid- ~~to~~ and far-infrared radiances during the WHAFFFERS campaign

Benedict Pery[1], Helen Brindley[1,2], Jonathan Murray[1,2], Sophie Mosselmans[1], Sanjeevani Panditharatne[3], Laura Warwick[4], Robin Hogan[3], Yi Huang[5], Benjamin Riot–Bretêcher[5], Hilke Oetjen[4], Dirk Schuettemeyer[4], and Tristan L'Ecuyer[6]

[1]Department of Physics, Imperial College London, UK
[2]National Centre for Earth Observation, Imperial College London, UK
[3]European Centre for Medium-Range Weather Forecasts, Reading, UK
[4]ESA/ESTEC, Noordwijk, the Netherlands
[5]Department of Atmospheric and Oceanic Sciences, McGill University, Canada
[6]Space Science and Engineering Center, University of Wisconsin-Madison, USA

Correspondence: Benedict Pery (b.pery24@imperial.ac.uk)

Abstract. Despite containing up to half of the Earth's thermal emission to space, the far-infrared spectral region (FIR, defined here as 100–667 cm^{-1} or 15–100 µm) has seldom been observed from satellites. This has contributed to substantial uncertainties in the spectroscopy of water vapour, radiative properties of clouds, and surface spectral emissivity; these in turn limit confidence in modelled FIR energy flows. With the advent of the Polar Radiant Energy in the Far-InfraRed Experiment (PREFIRE), a step is taken towards new, systematic, spectral observations of the Earth in the FIR. Launched in 2024, the two PREFIRE CubeSats offer a new perspective of Earth's outgoing longwave energy with moderate spectral resolution. However, the observational uncertainty budget requires further consolidation.

In this study we assess the accuracy of PREFIRE spectral measurements through a 'ground-to-space' closure experiment. Using zenith-viewing observations from the ground-based Far INfrarEd Spectrometer for Surface Emissivity (FINESSE) ~~, we gauge the representativity of atmospheric data~~ recorded during the WHAFFFERS campaign, we constrain atmospheric data taken from in situ sensors~~and reanalysis. With these~~ . With this optimised profile data we simulate PREFIRE-observed radiances for an overflight of our field site in eastern Canada. Simulations of the FINESSE radiances are in very good agreement with observations, while those from PREFIRE indicate some bias beyond the calculated uncertainties. We find that atmospheric water vapour specification, uncertain surface properties, and instrument noise dominate the uncertainties. Based on these findings, we highlight proposed techniques for closure experiments using terrestrial and satellite instruments alike. Such experiments will provide a ground-truth for validation of future FIR satellite missions.

1 Introduction

The interaction of thermal infrared radiation with Earth's atmosphere and surface plays a fundamental role in shaping the planet's weather and climate. Spectral observations in the thermal infrared can be used to retrieve atmospheric composition and temperature structure, and to understand the complex physics behind Earth system processes. Satellite observations additionally offer a powerful global view of these phenomena, and have been used for decades in the service of meteorology and atmospheric science.

The far-infrared (FIR), defined here as the region from 100–667 cm^{-1} (or 15–100 µm) comprises around half of the globally averaged longwave emission to space (Harries et al., 2008), and as such is a crucial component of the Earth's radiation budget. Water vapour is a key atmospheric absorber in the FIR, contributing to the significant FIR greenhouse effect (e.g. Sinha and Harries, 1995; Brindley and Harries, 1998). Conversely, in very dry and cloudless atmospheric conditions micro-windows 'open' in the FIR. These micro-windows comprise the FIR 'dirty window' region (here defined as 400–600 cm^{-1}), and permit radiation from the surface to escape to space. In this way, surface temperature and emissivity can also affect FIR measurements from space, as well as the top-of-atmosphere energy budget.

Ice clouds exert a strong influence in the FIR, with theoretical studies demonstrating substantial sensitivity of FIR radiances to the size and shape of ice crystals (Yang et al., 2003; Baran, 2007). More recent analyses using ground- and aircraft-based observations have confirmed this sensitivity and suggest that the region could provide uniquely powerful constraints on retrieved cloud properties (Maestri et al., 2014; Panditharatne et al., 2025; Di Natale et al., 2026).

Nevertheless, the scarcity of FIR observations (relative to other spectral regions such as the mid-infrared and microwave) means that significant uncertainties persist in fundamental gas spectroscopy (e.g. Mlawer et al., 2019), underlying ice optical properties and hence cirrus radiative properties (e.g. Wang et al., 2024; Bantges et al., 2020), and surface emissivity (e.g. Chen et al., 2014). These uncertainties can propagate into simulations of the future climate (e.g. Turner et al., 2012; Huang et al., 2018).

Despite its scientific importance, spectrally resolved observations of the FIR from satellites have been impeded by limitations of optical and sensor technology. The only such measurements until recently were from a sparse set of missions in the early satellite era (Hanel et al., 1971; Kempe et al., 1980). However, the launch of the Polar Radiant Energy in the Far-InfraRed Experiment (PREFIRE, L'Ecuyer et al., 2021) in 2024 marks the first step towards filling this FIR observational gap. This mission features two CubeSats launched as part of NASA's Earth Ventures initiative. A relatively low-cost mission, PREFIRE provides moderately resolved spectral radiances stretching into the FIR and aims to contribute to polar science at a time of rapid change in the polar climate. The radiances are used to retrieve temperature, water vapour, surface spectral emissivity, and spectral fluxes in clear-sky polar scenes, but a first step towards being confident in the accuracy of these retrievals is to have confidence in the radiances themselves.

Unbridled by the stringent requirements of a space mission, a limited set of accurate ground- and aircraft-based instruments observing the FIR has been available for some time. These instruments have furthered knowledge of the FIR radiative properties of several components of the Earth system, including water vapour (e.g. Mlawer et al., 2019) and the surface emissivity

(Bellisario et al., 2017; Murray et al., 2020). Zenith-pointing observations in clear sky have been used to profile the atmosphere with high accuracy, investigate downwelling radiance, and perform closure tests in the FIR (e.g. Mariani et al., 2012; Belotti et al., 2023; Mosselmans et al., 2026).

With the above in mind, in this work we carry out a radiative closure study in clear sky across the mid- to far-infrared, with a focus on the FIR. We use the FINESSE ground-based spectrometer (Murray et al., 2024) to ~~assess the representativity of~~ optimise atmospheric profiles gathered from ~~reanalysis and~~ in situ measurement. The high spectral resolution, accuracy, and known calibration of this spectrometer give us confidence in the accuracy of the atmospheric profiles and of our radiative transfer simulations. We then go on to compare simulations and measurements of satellite radiances from an overpass of the ground measurement site, serving to validate spectral radiance observations from PREFIRE and identify potential instrument biases. As far as we are aware, this work represents the first attempt to perform such an experiment in the far-infrared.

The layout of this paper is as follows. The data sources and methods used in the experiment are presented in Sect. 2. In Sect. 3, we discuss the various challenges to a rigorous radiative closure diagnosis, and present a detailed investigation into the sources of uncertainty in the experiment. We present results of the ~~closure experiment, both on the ground and in space,~~ ground-based closure experiment using FINESSE to optimise the input atmospheric profile in Sect. 4, and results of the space-based closure with PREFIRE in Sect. ~~?? and~~ 5. Finally, we discuss the findings in Sect. 6.

2 Data sources and methods

2.1 The WHAFFFERS campaign

The W-band, HiSRAMS, AERI, FIRR2, FINESSE and FIRMOS Experiment on Remote Sensing (WHAFFFERS) campaign was a multi-modal field study conducted in Canada, with sites in Ottawa and near Montreal, in January and February of 2025. Observations of the atmosphere and land surface were gathered simultaneously by passive and active instruments across the two sites and from an aircraft. Among the aims of the campaign was to investigate consistencies between radiometric instruments by performing radiative closure experiments. We investigate a closure experiment in this work with a focus on measurements from the research station at the Gault Nature Reserve of McGill University (45.535° N, 73.149° W). This site sits at c.130 m above sea level on the side of a forested hill, surrounded by mostly flat agricultural land at c.30 m above sea level.

Meteorological conditions were anomalously cold and dry in this region of Canada during the campaign which was ideal for study of the far-infrared; all radiosondes launched during the campaign measured a total column water vapour (TCWV) of less than 0.6 cm. The reduced optical depth of the atmospheric column in the FIR water vapour absorption features affords greater sensitivity than normal to higher altitudes and to water vapour spectroscopy when measured from the ground.

2.2 Spectral measurements

2.2.1 FINESSE

The Far-infrared Spectrometer for Surface Emissivity (FINESSE, Murray et al., 2024) is a ground-based radiometer developed at Imperial College, employing a commercial Bruker EM27 Fourier-transform spectrometer. FINESSE was originally configured to measure over the range 400–1600 cm^{-1} with a spectral resolution reaching 0.5 cm^{-1}. It features a custom front-end optics system that enables both the study of surface emissivity and zenith-looking views of the atmosphere. FINESSE has been used to retrieve surface emissivity under laboratory conditions (Warwick et al., 2024) and in the field (Warwick et al., 2025) using measurements from a campaign in Andøya, Norway in 2023. Measurements from this field campaign have also enabled study of the polar atmosphere (Mosselmans et al., 2026). The instrument is equipped with ancillary sensors to measure temperature, pressure, relative humidity, and CO_2 concentration.

Work has been ongoing since the Norway campaign to improve the FINESSE instrument. Replacing the liquid nitrogen cooling with a Stirling cooler has eliminated the need to interrupt measurements to perform dewar refills and extended the measurement range slightly further into the FIR, now reaching 380 cm^{-1}. ~~Vibrations induced by the Stirling cooler were removed outside of the required modulated frequency band by doubling the FINESSE scan speed , with~~ The scan speed of the instrument has also been doubled such that each interferometer scan ~~lasting~~ now lasts 0.75 s rather than the 1.5 s of the original configuration. ~~Intercomparison with a co-located AERI spectrometer during the WHAFFFERS campaign enabled the diagnosis and removal of a small bias between 1400–1600 . This bias was caused by internal reflections in the spectrometer assembly and had gone undetected in the Andøya FINESSE measurements.~~

2.2.2 PREFIRE

The Polar Radiant Energy in the Far-Infrared Experiment mission (PREFIRE, L'Ecuyer et al., 2021) consists of two 6U CubeSats in different near-polar Sun-synchronous orbits, each equipped with a Thermal Infrared Spectrometer (TIRS) instrument; the satellites were launched in May/June 2024. The TIRS is a lightweight grating spectrometer covering a spectral range of 5–54 µm (185–2000 cm^{-1}), with a nominal spectral sampling of ∼0.84 µm (equivalent to ∼5 cm^{-1} at 250 cm^{-1}, or ∼20 cm^{-1} at 500 cm^{-1}). The four order sorting filters used in the TIRS instrument split the measurements into four distinct spectral bands. In order of increasing wavelength, these bands are referred to as MIR-1, MIR-2, FIR-1, and FIR-2.

The TIRS grating separates incoming radiation from eight cross-track 'scenes' onto the uncooled detector array, where each scene has a full complement of detectors for all spectral channels. This results in different sensor noise characteristics for each cross-track view. On the Earth's surface, the scenes are non-contiguous and stretch across a 264 km swath, acting as an eight-toothed 'comb' moving along the satellite track. Each field of view (FOV) has a surface footprint of approx 11.8×34.8 km (cross- × along-track) with cross-track gaps between of approx 24.2 km. There is substantial overlap in the FOVs in the along-track direction, with any point along the orbit observed by up to 7 overlapping footprints. Note that these values will change as the satellites' orbits decay over the mission lifetime. A single spectrum of the TIRS instrument is recorded at each FOV.

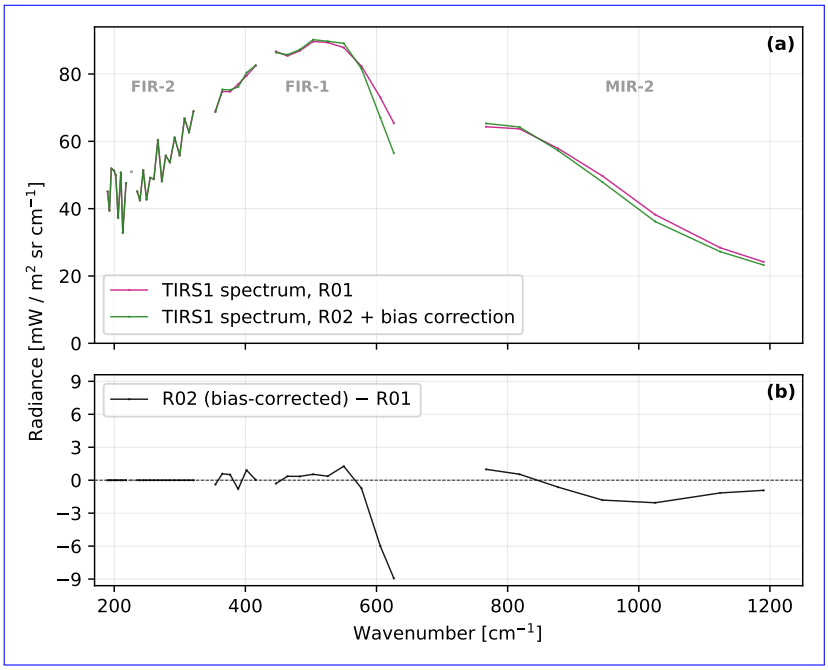


Figure 1. (a): Example PREFIRE TIRS 1 spectra (from across-track scene 6) for the first and second release (R01 and R02) of the Level 1 radiance product. The R02 spectrum includes the new bias correction term. Grey text labels the spectral bands of the TIRS instrument. **(b)**: Spectral differences between the two releases.

In the initial release (R01) of the PREFIRE level 1 radiance product (1B-RAD), the science team have identified discrepancies between the instrument model of the spectral response functions and the true instrument response. The second release (R02) of the L1B data includes an empirical correction factor for the spectral radiance. This correction can be added to the reported spectral radiance to account for these discrepancies, as is done for the analysis in this study. Figure 1 illustrates the effect of this correction on the spectra used in this study. The correction factor is derived using a combination of three distinct reference radiances: ~~IASI collocated spectra~~ collocated spectra from the Infrared Atmospheric Sounding Interferometer (IASI, Hilton et al., 2012) and Cross-track Infrared Sounder (CrIS, Han et al., 2013) instruments convolved to PREFIRE channels, ~~CrIS collocated spectra convolved to PREFIRE channels, and PCRTM~~ and Principal Component Radiative Transfer Model (PCRTM, Liu et al., 2006) modelled clear-sky radiances derived using the PREFIRE Auxiliary Meteorology product (Mattingly et al., 2025) as input. More details on this correction factor will be published in due course.

2.2.3 Selection of spectral data

FINESSE operated on 20 days across the WHAFFFERS campaign, collecting approximately 135 hours of measurements. During the FINESSE observation periods, PREFIRE FOVs with ~~valid spectra~~ spectra meeting quality control checks passed close to the site (within ∼25 km~~of) the site~~) on 7 occasions. A further 19 overpasses were not captured by FINESSE due to

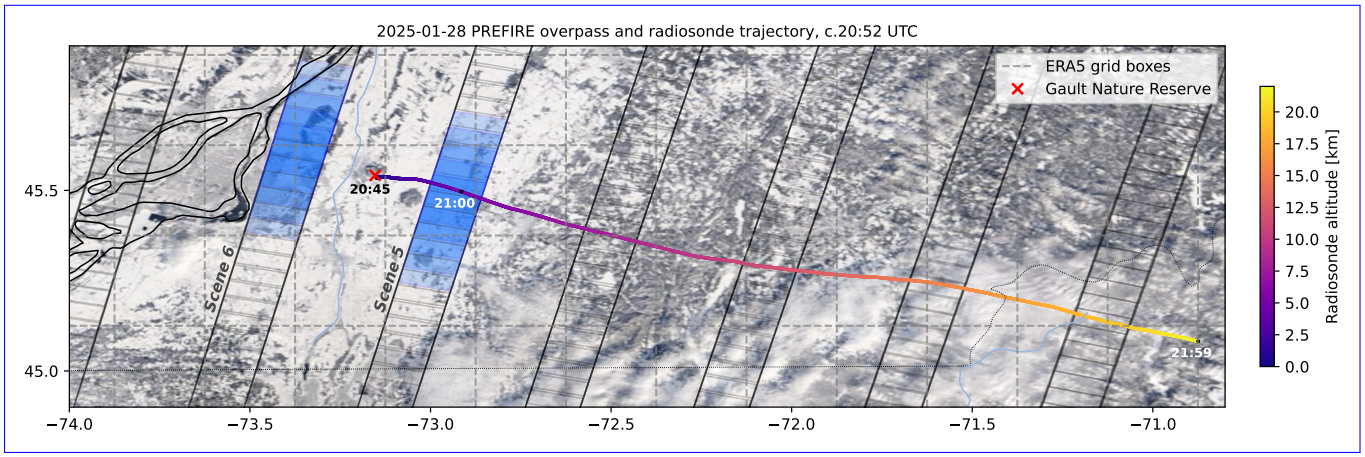


Figure 2. Map showing the layout of measurements for our case study. The red cross marks the the Gault Nature Reserve site, where FINESSE was located. The track of the radiosonde launched from here is shown, with times (UTC) labelled throughout the flight and colours indicating its altitude. Solid boxes across the image indicate the PREFIRE FOV polygons from the overpass, with significant overlap in the along-track direction (approx. north-east–south-west). FOVs selected for averaging in the scenes 5 and 6 are shaded blue. Grey dashed lines indicate the ERA5 grid boxes for reference. The background image is from MODIS Terra observations, approx 6 hours before the PREFIRE overpass (Credit: NASA).

either the time of the overpass (outside of working hours in the evening or at night) or weather conditions (FINESSE cannot operate during precipitation). Of the 7 captured, we focus on the PREFIRE satellite 1 overpass on 28th January 2025 at 20:52 UTC (15:52 local time). This case was the only one of these 7 to have verifiable clear skies throughout the observed scene and a radiosonde release at the time of the overpass.

For this study we average all spectra from a five minute window of the FINESSE measurements, centred on the PREFIRE overpass. FINESSE was continuously recording in zenith view mode and collected 400 interferometer scans in this time. The spectra ~~exhibit good stability~~ are stable over the measurement period, with their standard deviation equal to the FINESSE noise-equivalent spectral radiance (NESR), indicating no marked evolution in the atmospheric state. PREFIRE measurements are taken from the Level 1B-RAD product, version R02, with the bias correction factor included. Valid spectra from the overpass whose FOV midpoint was within 0.25° (latitude/longitude) of the Gault station are averaged along-track to yield two spectra for comparison, from the cross-track TIRS 1 scenes 5 and 6. All channels in the MIR-1 PREFIRE band have known calibration issues and so are neglected here.

2.3 Ancillary atmosphere and surface data

To model infrared radiative transfer in clear skies (that is, neglecting the contributions of cloud and aerosol), we require ~~temperature and gas concentrations~~ gas concentrations and temperature as functions of pressure or altitude. In the thermal infrared region we study here, encompassing 185–1600 cm^{-1} across both instruments, the dominant absorbing and emitting

species are water vapour, carbon dioxide, and ozone, with other trace gases such as methane and nitrous oxide also required to simulate spectral radiance with high accuracy. The spectral emissivity and radiating temperature of the surface are needed in addition to simulate infrared radiation upwelling to space.

For this study, we make use of a range of atmospheric data sources. Firstly~~we use ERA5 hourly profiles of temperature, specific humidity, and ozone concentration as a function of pressure on 137 atmospheric model levels, at a horizontal resolution of 0.25° (Hersbach et al., 2020). We also use the corresponding ERA5 estimates of the surface skin temperature (T_{sfc}).~~

~~Secondly,~~ , we use radiosondes launched periodically during the WHAFFFERS campaign ~~also~~ which measured profiles of temperature and humidity. The radiosonde model used during WHAFFFERS was the InterMet Systems iMet-4 radiosonde. In the literature, we found limited prior studies using this model (see e.g. Ghysels et al., 2024; Liu et al., 2024) or brand (Hurst et al., 2011; Flores et al., 2013); its performance has not been independently and systematically reviewed. Figure 2 shows the track of the radiosonde launched at 20:45 UTC on 28th January 2025, with the PREFIRE observation footprints from the c.20:52 UTC overpass overlaid. Temperature, relative humidity, altitude, and pressure measured by the radiosonde are available at 5 m vertical intervals. Radiosonde data are smoothed before input into the radiative transfer model.

~~Finally~~Secondly, during the WHAFFFERS campaign, near-surface meteorological data were recorded continuously at the Gault Nature Reserve at a weather station within 50 m of FINESSE. ~~Measurements of relevance to our study are from eight~~ We use measurements from four Vaisala HMP155A probes at ~~different~~ heights up to 10 m above ground, with temperature and relative humidity readings taken every minute. ~~Analysis of these data over several measurement days indicated that probes at 1.5 and 3.5 above ground level were consistently biased and so their readings have been discarded.~~ Thirdly, we use ERA5 hourly profiles of ozone concentration as a function of pressure on 137 atmospheric model levels, at a horizontal resolution of 0.25° (Hersbach et al., 2020). ERA5 profiles of temperature and specific humidity also supplement data from the radiosonde outside of its vertical extent.

~~The emissivity of the surface ($\varepsilon_{\mathrm{sfc}}$) is taken from the dataset compiled by Huang et al. (2016) which provides modelled estimates of spectral emissivity at nadir-view for a variety of surface types and is the only dataset to offer this into the far-infrared. The 'medium snow' surface type (with median grain size 600) is used in this study; fine and coarse snow as well as ice surface types are also available.~~

Finally in the setup of the simulated atmosphere, key trace gases are specified as follows. Concentrations of CO_2, CH_4, and CO are taken from the CAMS global greenhouse gas forecasts (Agustí-Panareda et al., 2019). For N_2O and SF_6, we take mixing ratios from NOAA's Global Monitoring Laboratory (NOAA), while for CFC-11, CFC-12 and CCl_4 concentrations are estimated by extrapolating the average 5-year trend of Atmospheric Histories (Bullister and Warner, 2017). Mixing ratios of the latter five greenhouse gases are assumed constant with height.

The ~~different sources of atmospheric data are combined to generate profiles specifically for downwelling (FINESSE) and upwelling (PREFIRE) radiance simulations. To probe the impact of the characterisation of the atmosphere on the associated radiances, in each case we create two sets of temperature and humidity profiles~~emissivity of the surface ($\varepsilon_{\mathrm{sfc}}$) is taken from the dataset compiled by Huang et al. (2016) which provides modelled estimates of spectral emissivity at nadir-view for a variety of surface types and is the only dataset to offer this into the far-infrared. The '~~ERA5' set is based purely on the closest ERA5~~

profile in space and time (45.5° medium snow' surface type (with median grain size 600 N, 73.25° W, μm) is used in this study; fine and coarse snow as well as ice surface types are also available.

Surface temperature is estimated using the GOES-16 Advanced Baseline Imager's (ABI) full-disk land surface temperature retrieval (ABI-L2-LST, GOES-R Algorithm Working Group and GOES-R Series Program, 2018). This is sampled at 21:00 UTC) , while the 'in-situ' set is based primarily on the available in situ measurements. Table ?? provides a summary of the inputs to each set and the associated nomenclature we use to refer to each simulation. Apart from atmospheric temperature and humidity, all components described above are specified identically for the ERA5 and in-situ simulations.The same surface and atmosphere is used to simulate both TIRS scenes 5 and 6.

The only difference between the ERA5-DW and ERA5-UW profile is the choice of the lower boundary. For the former, we take the observation level as 130UTC, just seven minutes after the PREFIRE overpass, and has a 10 above sea level, consistent with FINESSE's altitude on a hillside at the Gault site. For the latter we use the entire ERA5 vertical profile (which has a surface altitude of 30) . There are more substantial differences between the in-situ-DW and in-situ-UW cases. For the former we replace the radiosonde profile between 130–140 with values from the weather station tower. For the latter, we do not use the weather station measurements and instead supplement the radiosonde values with co-located ERA5 data between 130 and the surface. Similarly, in both cases, at altitudes above the maximum extent of radiosonde measurements we add the ERA5 data.The radiosonde data used in the in-situ profiles is smoothed from its native 5 resolution before simulation. km resolution at nadir. For each TIRS scene, we take an average of the ABI retrieved land surface temperature values within the TIRS FOV polygons, weighted by area and overlap fraction.

Data sources used to specify temperature and water vapour concentration across altitude regimes (left-hand column) for the different atmospheric profiles simulated. Simulated surface properties are also shown for PREFIRE observations. The marking "—" indicates that no simulation of this level was performed in this case. Specification of other gases is identical across the four profiles and is detailed in the text. Instrument FINESSEPREFIRE Profile shorthand ERA5-DWIn-situ-DW ERA5-UW In-situ-UW >21.8 ERA5 ERA5 140 –21.8 Radiosonde (smoothed)130–140 Weather station<130 — — ERA5 Surface — — T_{sfc}: ERA5; ϵ_{sfc}: Huang et al. (2016)

Temperature and water vapour mixing ratio profiles for the ERA5 and in-situ cases are shown in Fig. 3. The unadjusted input profile from the above sources is represented as profile 'A'. The insets highlight the near-surface conditions crucial for simulating FINESSE measurements. The profiles of temperature are broadly similar, with some differences reaching up to 5 in parts of the free troposphere. The near-surface temperatures measured by the radiosonde immediately after launch are around 0.5–1 warmer than the corresponding ERA5 values, behaviour which is not seen in the weather station observations. This does lead to a distinct feature in the in-situ-UW profile where the ERA5 and radiosonde profiles are joined, but sensitivity studies confirmed this has negligible impact on simulated upwelling radiances at the top of the atmosphere. The two water vapour profiles are more different; while both show a moist layer of similar extent at c.500 , water vapour varies significantly below that. Overall, the in-situ profiles indicate a drier atmosphere. , and the values of total column water vapour (TCWV) are included as annotations.

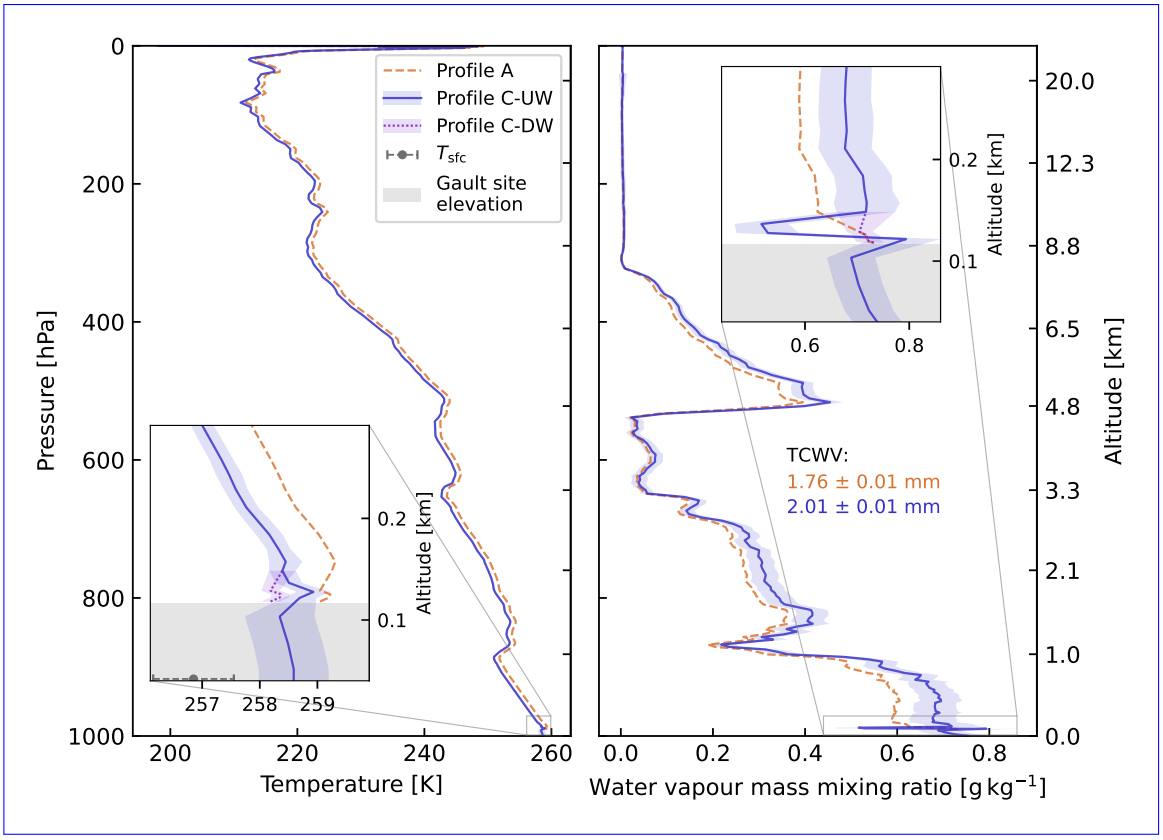


Figure 3. Profiles of temperature (left) and water vapour (right) for the ~~cases simulated~~profiles A and C, with coloured shading showing the ~~respective~~ uncertainties for profile C. The ~~ERA5-DW~~ C-DW and ~~-UW profiles use~~ C-UW simulations have slight differences in the ~~same data~~near-surface atmosphere shown in the inset. ~~The dotted line indicates where~~ Profile B comprises the ~~in-situ-DW~~ temperatures of profile ~~differs from~~ A with the ~~in-situ-UW~~ water vapour specification of profile ~~; above this, the two in-situ profile specifications are identical~~C. Grey shading in the ~~inset plots~~ insets indicates the elevation of the Gault site~~; data below this is neglected for downwelling (DW) simulations. The skin temperature from ERA5, used in both upwelling simulations, is shown in~~ while the temperature inset plot also shows the simulated surface skin temperature. Colour-coded text shows the total column water vapour (TCWV) for ~~ERA5-UW~~ the A and ~~in-situ-UW~~ C profiles (right).

2.4 Radiative transfer modelling

Simulated radiances at the top of atmosphere and at the surface are generated using the Line-by-Line Radiative Transfer Model (LBLRTM, Clough et al., 2005). Its high accuracy has led to it becoming a standard benchmark for spectrally resolved radiative closure experiments (e.g. Delamere et al., 2010; Sussmann et al., 2016; Mlawer et al., 2019) and for evaluation of other radiative transfer codes (e.g. Oreopoulos et al., 2012; Hogan and Matricardi, 2020). For this work, we use LBLRTM v12.17, including spectral lines from AER Line File v3.8.1, and the MT_CKD v4.3 water vapour continuum model (Mlawer et al., 2023).

We input ~~the profiles~~ profiles based on the data sources described in Sect. 2.3 to LBLRTM, simulating the effects of the first 30 molecules listed in the HITRAN database. For those gases not ~~mentioned above~~explicitly mentioned in Sect. 2.3., we use the LBLRTM 'mid-latitude winter' default values.

To simulate the PREFIRE and FINESSE measurements, instrument characteristics must be applied to the very high resolution radiances calculated by LBLRTM. For PREFIRE, the radiance from each channel of the grating spectrometer is calculated by integrating the LBLRTM output with the normalised channel spectral response function ~~(v13, ?)~~(v13, Drouin et al., 2025a). To simulate FINESSE radiances, spectra are converted to interferograms and truncated to mimic the effects of an ideal Fourier-transform spectrometer with FINESSE's maximum optical path difference. After converting the truncated interferograms back to spectra, they are convolved with a spectrally dependent instrument line shape as described by Murray et al. (2024), which simulates asymmetries in FINESSE's optical path.

3 Uncertainties and challenges in closure analysis

3.1 Instrument performance

Uncertainties in FINESSE radiances are well-characterised and fully described by Murray et al. (2024). Briefly, the noise-equivalent spectral radiance (NESR) is a random error resulting from spectrally uncorrelated detector noise and can be reduced through averaging, while other (systematic) uncertainties arise from the calibration process. For the measurement conditions of our study, these are both shown in Fig. 4a.

Uncertainties in the PREFIRE radiances are quantified as noise-equivalent radiances, shown in Fig. 4b. Some elements of the detector array are known to have high noise or responsivity faults and we have masked their readings. This leads to some gaps in the FIR spectra. Channels in the FIR-2 band are flagged as having 'uncategorised calibration' due to uncharacterised instrument issues. Uncertainty in PREFIRE calibration (i.e. absolute radiometric accuracy) is not known. Information on PREFIRE observational issues identified prior to launch is detailed by Drouin et al. (2025b), and post-launch in section 4 of the PREFIRE radiance product R01 user guide (Hokanson Wagner et al., 2025).

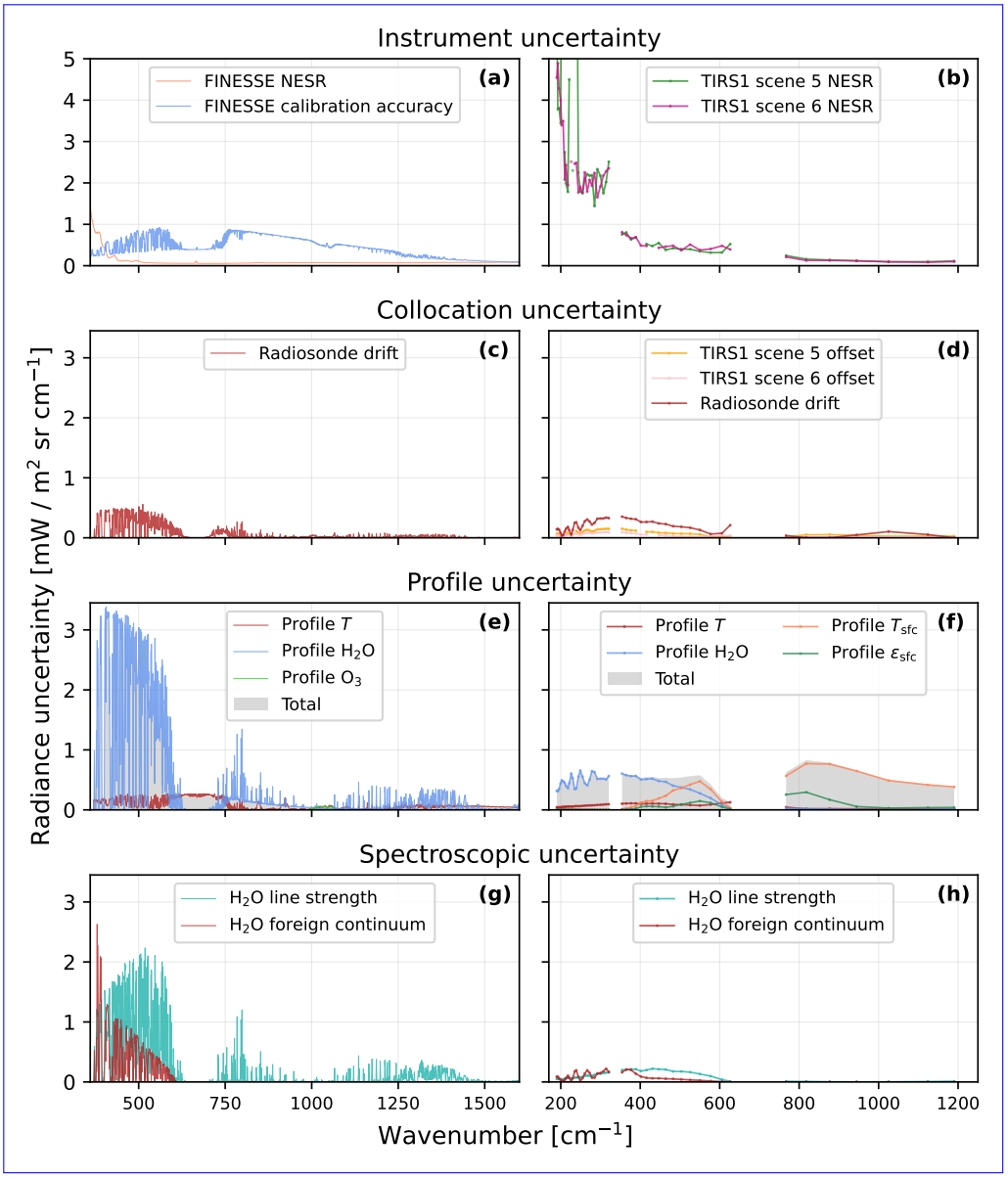


Figure 4. Estimates for the sources of uncertainty considered in the closure experiment. The left column **(a, c, e, g)** is for FINESSE, the right **(b, d, f, h)** for PREFIRE. **(a, b)**: uncertainty in measured radiances due to instrument noise (NESR) and calibration. **(c, d)**: uncertainty estimate due to inexact collocation of sensors. **(e, f)**: 1-σ uncertainty in simulated radiances due to uncertainty in the various labelled profile quantities. **(g, h)**: uncertainty in simulated radiances following from uncertain H_2O spectroscopic parameters. Note the different y-scale used in **(a, b)** compared to other rows.

3.2 Spatial collocation

In the discussion of the experimental setup thus far we have assumed that all data sources and instruments describe or measure the same atmospheric column. Since this is not the case, we examine here the effect of imperfect horizontal collocation in our measurements.

We use ERA5 fields to estimate the spatial variability in the scene meteorology at scales larger than the ERA5 horizontal scale of 0.25°. In the absence of horizontal wind, the radiosonde would sample only the atmospheric column immediately above FINESSE. In reality, the wind advects the radiosonde some 185 km east of the Gault reserve over its flight ~~.~~ (see Fig. 2). We construct a profile which ~~'follows' the radiosonde trajectory and~~ samples from the spatially and temporally closest ERA5 grid cells ~~(termed 'ERA-following-sonde' as shorthand)~~tracking the radiosonde trajectory, assuming that the ERA5 fields are representative of the true spatial variability of the scene meteorology. The radiances from this profile are simulated as described in section 2 and compared to those using ~~the standard~~ a single-column ERA5 profile; ~~this comparison is shown~~ the modulus of this difference is considered as an uncertainty estimate for this drifting effect and is shown as 'radiosonde drift' in Fig. ~~??a and b. This offset is included as an uncertainty for the in-situ simulations.~~ 4c–d.

As demonstrated in Fig. 2, the PREFIRE FOVs 5 and 6 lie either side of the Gault site, and so do not pass directly over FINESSE. To assess the impact this has, we simulate the radiances from the atmospheres of ERA5 grid points contained in the PREFIRE footprints ~~. The comparison~~ while controlling for the surface temperature. The average of offsets between these and radiances simulated from the closest grid point to the Gault site is ~~shown~~ plotted as 'scene offset' lines in Fig. ~~??. The average of these offsets, weighted by the number of FOV midpoints falling in each box,~~ 4d. This is included as an uncertainty ~~source~~ estimate for the PREFIRE simulations.

~~Top row: differences in simulated FINESSE (a) and PREFIRE (b) radiances when using a profile of ERA5 data 'following' the radiosonde track, compared to a single ERA5 column at the Gault site. Bottom row: differences in simulated PREFIRE radiances for TIRS scene 5 (c) and 6 (d) simulated using various ERA5 grid points located within the instrument FOV, compared to that closest to the Gault site (45.5° N, 73.25° W).~~

3.3 ~~Instrument performance~~

~~Estimates for several sources of uncertainty considered in the closure experiment. The left column (a, c, e, g) is for FINESSE, the right (b, d, f, h) for PREFIRE. (a, b): uncertainty in measured radiances due to instrument noise and calibration. (c–f): uncertainty in simulated radiances due to uncertainty in the various labelled profile quantities; the legends in (c) and (d) apply also for (e) and (f) respectively. (g, h): uncertainty in simulated radiances following from uncertain spectroscopic parameters; the legend in (g) applies to both plots. Note the different y-scale used in (a, b) compared to other rows. Uncertainties in FINESSE radiances are well-characterised and fully described by Murray et al. (2024). Briefly, the noise-equivalent spectral radiance (NESR) is a random error resulting from spectrally uncorrelated detector noise and can be reduced through averaging, while other uncertainties arise from the calibration process. For the measurement conditions of our study, these are both shown in Fig. 4a.~~

~~Uncertainties in the PREFIRE radiances are quantified as noise-equivalent radiances, shown in Fig. 4b. Some elements of the detector array are known to have high noise or responsivity faults and we have masked their readings. This leads to some gaps in the FIR spectra. Channels in the FIR-2 band are flagged as having 'uncategorised calibration' due to uncharacterised instrument issues. Uncertainty in PREFIRE calibration (i.e. absolute radiometric accuracy) is not known. Information on PREFIRE observational issues identified prior to launch is detailed by Drouin et al. (2025b), and post-launch in section 4 of the PREFIRE radiance product R01 user guide (Hokanson Wagner et al., 2025).~~

3.3 Constraining atmospheric and surface states

Quantification of the uncertainty in the input atmosphere and surface profiles varies by data source. ~~For ERA5 data, we represent the uncertainty in reanalysis quantities using the standard deviation of the accompanying 10-member ensemble.~~ Uncertainties in readings from the radiosonde and weather station are calculated using information from the respective manufacturers' data sheets (InterMet Systems, 2022; Vaisala, 2025). 'Calibration uncertainty' or 'repeatability in calibration' figures are treated as systematic uncertainties and 'accuracy' or 'combined uncertainty' figures as random uncertainties. ~~Surface emissivity uncertainty~~ For ERA5 data, we represent the uncertainty in reanalysis quantities using the standard deviation of the accompanying 10-member ensemble. The surface temperature uncertainty estimate takes the precision of the ABI land surface temperature retrieval identified by Yu and Yu (2020), while uncertainty in surface emissivity is estimated as the ~~spectrally averaged~~ spread in the fine, medium, and coarse snow types in the Huang et al. (2016) dataset. These uncertainties encompass temperature, humidity, ozone concentration, surface temperature, and surface emissivity; uncertainty in other quantities supplied to the radiative transfer code is considered negligible. Uncertainty estimates for temperature, water vapour mixing ratio, and T_{sfc} are shown in Fig. 3.

For a simulated total state vector $\boldsymbol{x}$, the uncertainties described above may be represented as a pair of vectors $(\boldsymbol{\sigma}, \boldsymbol{s})$ of random and systematic errors respectively. These vectors have components (σ_i, s_i) for the level i where s_i may be zero if there is no systematic uncertainty considered. We tackle random and systematic uncertainties separately and add them to calculate a sample set of realistic ~~errors~~ error perturbations in the total state vector~~, represented $\delta_m \boldsymbol{x}$~~ : $\delta_m \boldsymbol{x} = \delta_m \boldsymbol{x}_{\mathrm{sys}} + \delta_m \boldsymbol{x}_{\mathrm{rand}}$ (the m subscript labelling the samples). ~~For random errors , we construct a covariance matrix such that they~~ Assuming the random errors are correlated between nearby atmospheric levels~~. This~~ , we construct a covariance matrix $\mathbf{C}$ ~~has terms defined by~~ of the form:

$$C_{ij} = \sigma_i \sigma_j \exp\left(-\frac{|z_i - z_j|}{h}\right), \tag{1}$$

with z_i the altitude of level i and h some vertical correlation scale height (Rodgers, 2000; Feldman et al., 2008). ~~Sample random profile~~ Profile perturbations due to random errors $\delta_m \boldsymbol{x}_{\mathrm{rand}}$ are ~~randomly~~ sampled from a multivariate normal distribution with mean ~~$\boldsymbol{\sigma}$~~ $\mathbf{0}$ and covariance $\mathbf{C}$. Conversely, systematic errors are modelled as fully vertically correlated. In practice, this means that sample ~~systematic profile errors $\delta_m \boldsymbol{x}_{\mathrm{sys}} = z_m \times \boldsymbol{s}$, with~~ perturbations due to systematic errors $\delta_m \boldsymbol{x}_{\mathrm{sys}} = z_m \boldsymbol{s}$, with the values z_m sampled from a standard normal distribution. ~~These random and systematic sources are then added for each sample: $\delta_m \boldsymbol{x} = \delta_m \boldsymbol{x}_{\mathrm{sys}} + \delta_m \boldsymbol{x}_{\mathrm{rand}}$.~~

Using LBLRTM, the Jacobian $\mathbf{J}$ is then evaluated as $J_{ij} = \frac{\partial y_i}{\partial x_j}$ for a spectral point i and some state variable x_j at layer j. This Jacobian encodes how a spectrum $\boldsymbol{y}$ responds linearly to some small change in the state vector $\boldsymbol{x}$. The instrument response is applied to the ~~output~~ high-resolution Jacobians output from LBLRTM as described in Sect. 2.2. Sample profile ~~uncertainties~~ perturbations $\delta_m \boldsymbol{x}$ are propagated to sample spectral ~~uncertainties~~ perturbations $\delta_m \boldsymbol{y}$ using $\delta_m \boldsymbol{y} = \mathbf{J}\, \delta_m \boldsymbol{x}$. The overall spectral uncertainty $\delta \boldsymbol{y}$ is calculated as the standard deviation of the perturbations $\delta_m \boldsymbol{y}$, using 5000 samples. This is repeated for each variable considered. For FINESSE these variables are temperature, and water vapour and ozone concentrations. We found that PREFIRE had ~~little~~ negligible sensitivity to ozone concentration uncertainty, so we consider temperature, water vapour concentration, surface temperature and emissivity.

The ~~in-situ profiles have~~ radiosonde profile has a significant error contribution from systematic uncertainties which dominates over random uncertainties; as such ~~these profiles have little sensitivity to the choice of h. We found some~~ the profile has modest sensitivity to the choice of h~~for the ERA5 profile uncertainty, having only random errors. For a similar quantity to h in the literature, Rodgers (2000, Ch 2) use the atmospheric scale height and Ridolfi et al. (2022) use a 5~~. Investigating across a range from 0.2–8.5 km~~correlation in retrieval covariances, Warwick et al. (2022) find a vertical correlation length of 0.8 for temperature and water vapour in the Met Office UM, and from measurements Fischer et al. (2013) suggest a non-convective water vapour correlation of 0.23 . Investigating across this range~~, we found that radiance uncertainties due to water vapour errors varied by ~~a factor of 3~~less than 25 %; we choose a value of h =1.5 km for temperature and water vapour in this work, representing a slightly conservative middle ground. The resulting uncertainties in simulated radiances represent a 1-σ uncertainty bound and are shown in Fig. 4~~c–f~~e–f.

3.4 Water vapour spectroscopy

Since we use a relatively fine vertical resolution and perform line-by-line calculations, the most significant uncertainties in the radiative transfer forward modelling come from either the input spectroscopic data or in the assumptions used to model spectroscopic phenomena such as spectral line mixing. We neglect investigation of line mixing uncertainty and instead focus on the uncertainty from water vapour spectroscopy as the dominant and most variable absorber in this case. In particular, we consider uncertainties in H_2O line strengths and in the absorption coefficients of the FIR components of the H_2O foreign continuum, similar to Mosselmans et al. (2026). We found that uncertainties in the line positions had a negligible effect on the simulated spectra. We also neglect any uncertainties in absorption coefficients for other parts of the water vapour continuum, as (a) foreign continuum absorption is substantially smaller at larger wavenumbers, and (b) the self-continuum absorption will be small anyway in this case due to the very dry atmosphere.

Water vapour line strengths are perturbed according to the assigned uncertainty code in the AER Line File, while foreign-continuum absorption coefficients are perturbed by the uncertainty values assigned by Mlawer et al. (2019). LBLRTM is then re-run using this perturbed spectroscopy. The resulting difference of this compared to a simulation with unperturbed spectroscopy is taken as the spectral uncertainty due to spectroscopic uncertainties. These uncertainties are presented in Fig. 4g and h.

~~In our results, we combine the spatial collocation, instrument, forward-modelled profile, and spectroscopic uncertainties in quadrature to form a total uncertainty for each of the four simulations.~~

4 Optimising ground-based closure

5 ~~Results~~

To assess radiative closure, we subtract the spectra measured by ~~the FINESSE and PREFIRE TIRS instruments~~ FINESSE from the spectra simulated as described in sections 2.3 and 2.4. This difference is termed a 'residual', representing the offset of ~~measurements from simulations~~ simulations from observations. These residuals are compared to the bounds given by ~~the total uncertaintiescalculated in~~ total uncertainties, calculated by combining in quadrature the instrument, spatial collocation, forward-modelled profile, and spectroscopic uncertainties (all from Sect. 3~~. **(a)** FINESSE observations (black) and the in-situ-DW simulation for comparison. **(b)**: residuals for the ERA5-DW simulation compared to observations. The grey shading and line indicate the total uncertainty limits described in Sect. 3. **(c)**: as in **(b)**, but for the in-situ-DW simulation.~~) for each simulation.

~~We begin by discussing residuals for the FINESSEinstrument, shown in Fig. 5. In these cases,~~ For FINESSE, a positive residual at some frequency indicates more emission by the overlying atmosphere in the simulation than was recorded in reality. For the viewing geometry here, this typically means either too much gas and/or too warm an atmospheric temperature; the inverse is true for negative residuals.

~~In both FINESSE cases, the residuals are generally close to zero throughout and mostly within the bounds of the uncertainty, indicating good agreement between observations and simulations. A large negative spike around 597.6~~As an initial profile (labelled 'A'), we take the reported radiosonde temperature and humidity, supplemented for FINESSE with the near-surface data recorded by the weather station. This profile is marked with orange dashes in Fig. ~~is attributed to deficiencies in the LBLRTM line coupling modelling used for and has been noted in other studies (e.g. Delamere et al., 2010; Mosselmans et al., 2026).We expect that the negative spike at 392~~3. The residuals for the FINESSE simulation using this profile are shown in Fig. ~~is related to the higher instrument noise at the edge of the FINESSE detection capability.A large positive spike at 667 is caused by the absorption and emission of the molecule; at this frequency it is so strong that only the cold air inside the instrument is sensed. Nearby wavenumbers are also quite opaque, so the positive bias of this feature in both ERA5 and in-situ profiles indicates that near-surface atmospheric temperatures are too warm in the simulated profiles~~5b. Residuals are generally close to zero throughout and mostly within the bounds of the uncertainty.

In the mid-infrared (for FINESSE, 667–1600 cm^{-1}) outside of the influence of CO_2, ~~the FINESSE residuals in both cases~~ residuals for profile A are very small and close to zero, without notable excursions from the uncertainty bounds. There is little downwelling radiance in the region, but the small residuals point towards a reasonably good specification of methane (1200–1400 cm^{-1}) and water vapour (1300–1600 cm^{-1}). Within the infrared window, agreement around the ozone absorption band (1000–1100 cm^{-1}) implies an accurate specification of ozone concentrations and upper-atmospheric temperatures. A very small negative bias within the uncertainty bounds is noted throughout the atmospheric window; this could be caused by emission from aerosols ~~or trace species which are~~ which is not simulated.

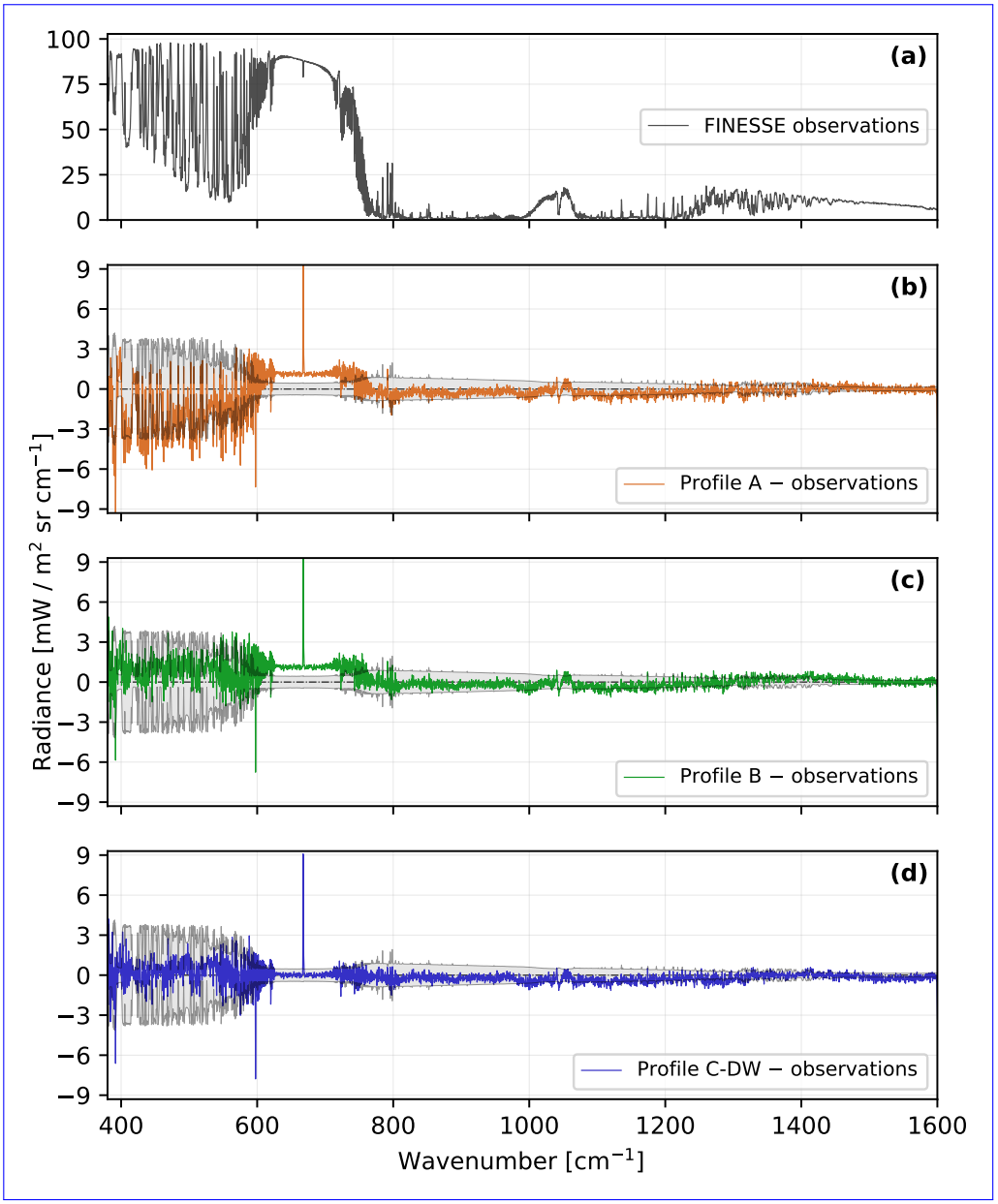


Figure 5. (a) FINESSE observed spectrum for the case study. (b–d): residuals (simulations−observations) for FINESSE simulations using profiles A, B, and C respectively. The differences between profiles are described in the text. The grey shading and line indicate the total uncertainty limits described in Sect. 3.

In the far-infrared, the ERA5-DW residuals are almost entirely within the uncertainty bounds. The slight positive bias in this region strongly affected by water vapour would suggest the simulated profile having slightly too warm or moist conditions, especially near the surface. Having too high a simulated near-surface temperature would be consistent with the However, there are two noteworthy regions where agreement is weaker for profile A. Firstly, there is a significant positive residual in the (620–720 cm^{-1}) CO_2 spectral feature. We note an unexplained deviation beyond the uncertainty limits around 395 but this is likely due to instrument noise, again being on the edge of the detection range.

The in-situ-DW , which suggests that the near-surface temperature simulated is warmer than that of the atmosphere observed by FINESSE. Secondly, residuals in the FIR have a negative bias, with the residual for many wavenumbers lying below the lower uncertainty boundfor this case. We conclude from the spectral range of this bias, the profile . This, when considering the previous issue, indicates that there is insufficient water vapour in the simulated profile compared to what is observed.

To remedy the issue in the FIR, we apply a scalar adjustment of the radiosonde-measured water vapour mixing ratio values to match the total water vapour column of ERA5. The scale factor required for this is 1.149 ± 0.028, which we applied as a whole-profile adjustment. The resulting profile 'B' is then simulated, and residuals are shown in Fig. 3, and the near-surface warmbias of the simulated atmospherediagnosed from the 5c. This adjustment leaves most FIR residuals now inside the uncertainty bounds, with a slight positive bias that supports the hypothesis that the modelled profile is too warm.

The issue in the 620–720 cm^{-1} region is addressed by modifying the temperature profile of the input atmosphere. We initially suspected that it would be sufficient to reduce temperatures in the lower troposphere, but it was found that the best agreement across the CO_2 emission feature , that this FIR negative bias spectral feature was achieved by modifying the entire profile by a fixed temperature offset. This offset was determined as 0.859 ± 0.109 K by inspecting brightness temperature residuals at the centre of the CO_2 band (the region 635–700 cm^{-1}). Applying this modification results in profile 'C-DW', shown as a solid blue and dotted purple lines in Fig. 3; we use 'DW' to distinguish the lower section of this profile, used to simulate downwelling radiance, to that used for simulating upwelling radiance. The resulting radiance residuals are found in Fig. 5d and demonstrate a much improved radiative closure agreement, only rarely deviating from the uncertainty bounds.

For all simulated profiles, a large positive spike in residuals at 667 cm^{-1} is caused by the radiosonde recording less total water vapour than is present in the atmosphere. absorption and emission of the CO_2 molecule; at this frequency it is so strong that only the cold air inside the instrument is sensed. A negative spike around 597.6 cm^{-1} is attributed to deficiencies in the LBLRTM line coupling modelling used for CO_2 and has been noted in other studies (e.g. Delamere et al., 2010; Mosselmans et al., 2026) . We expect that the negative spike at 392 cm^{-1} is related to the higher instrument noise at the edge of the FINESSE detection capability.

5 PREFIRE radiative closure results

Having constrained the atmospheric state with FINESSE in the previous section, we go on to use profile C to evaluate agreement of PREFIRE observations with simulations. We construct a profile 'C-UW', which has the same modified temperature and humidity profile as C-DW, but does not use weather station data near the surface and supplements the radiosonde profile

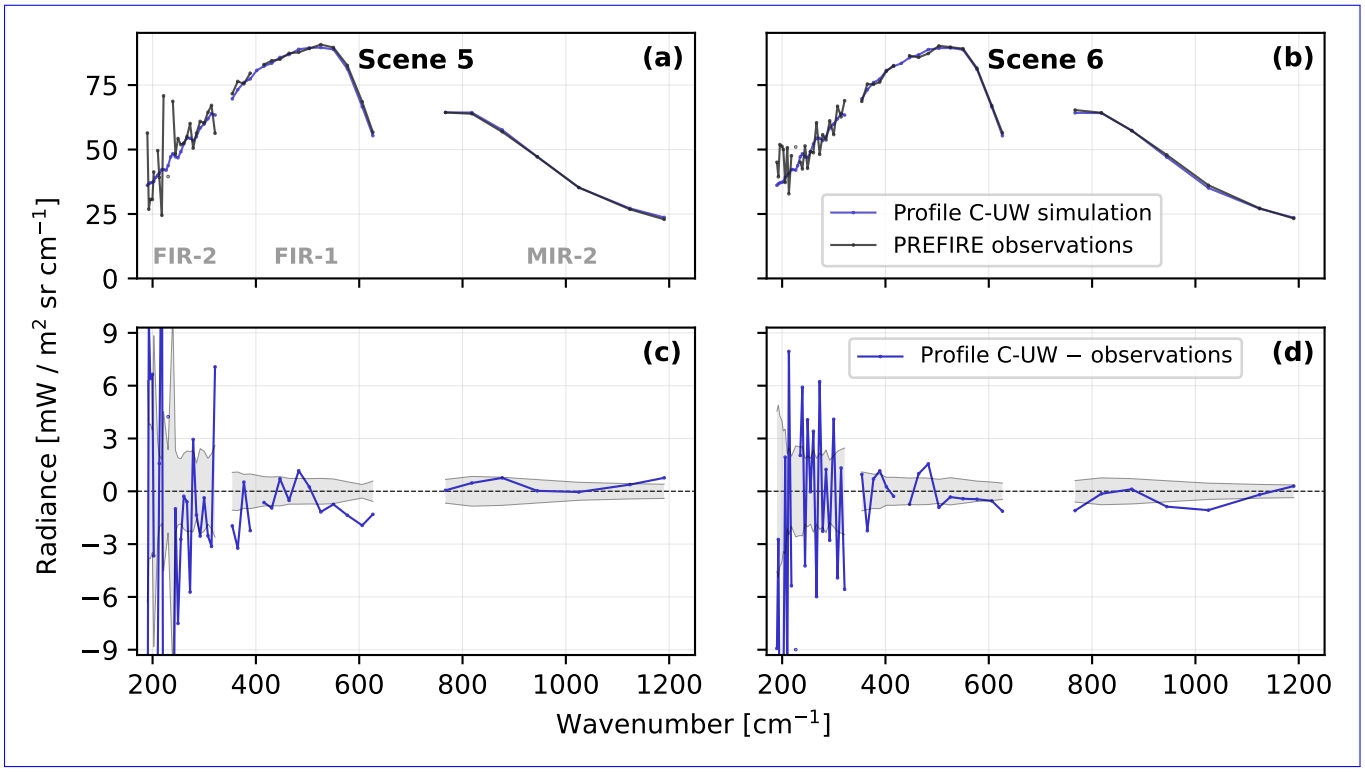


Figure 6. **(a, b)** PREFIRE observations (black) and the ~~in-situ-UW~~ profile C-UW simulation for comparison. **(c, d)**: residuals (simulations − observations) for the ~~ERA5-UW~~ profile C-UW simulation~~compared to observations~~. ~~Additional dashed lines indicate residuals for a simulation using land surface temperature observations from the ABI on GOES-16.~~ The grey shading and line indicate the uncertainty limits described in Sect. 3. ~~**(e, f):** as **(c, d), but for the in-situ-UW simulation.**~~ The left column ~~**(a, c, e)**~~ **(a, c)** shows the TIRS scene 5 radiances, and ~~**(b, d, f)**~~ **(b, d)** shows TIRS scene 6. The grey text in **(a)** labels the spectral bands of the TIRS instrument.

with ERA5 data between the surface altitude of the grid-box and the radiosonde launch altitude. It also includes the surface temperature and emissivity as described in Sect. 2.3. The profile is shown as solid blue throughout in Fig. 3.

The PREFIRE residuals are calculated as for FINESSE. Observed and residual PREFIRE spectra are shown in Fig. 6~~are~~, separated by cross-track TIRS scene to account for the different sensor characteristics, viewing angle, ~~and FOV geographies~~FOV geographies, and modelled surface temperatures. Here, a positive residual may indicate the simulation has too warm or emissive a surface or atmospheric layer, or too transparent an atmosphere (transmitting more radiation from warmer levels below and from the surface than in reality). In spectral regions common to both instruments, the PREFIRE residuals generally have a slightly larger magnitude, and much greater spectral variation, compared to FINESSE residuals degraded to PREFIRE spectral resolution (not shown). The effect of the large instrument noise in the FIR-2 band (185–330 cm^{-1}) is clear, with significant scatter even after averaging over five spectra.

The features of the residuals in the MIR-2 band show little difference between the ERA5-UW and in-situ-UW simulations; this is to be expected, as the simulations have identical specification of surface temperature, surface emissivity, and ozone concentrations. These are the main factors controlling radiances in this region under these conditions. The MIR-2 residuals exhibit a similar pattern in both cross-track scenes, with a slight spectral zig-zagging. In all comparisons residuals are positive in this region indicating too much modelled radiation from the surface, indicating either too warm or too emissive a surface in the simulationsScene 5 shows a strong agreement here, while in scene 6 some channels' residuals lie below the uncertainty bands, suggesting the surface temperature or emissivity is slightly underestimated.

Turning to the far-infrared bands, the difference between the ERA5-UW and in-situ-UW simulations becomes somewhat clearer. For both scenes in the dirty window (FIR-1 band), the ERA5-UW residuals lie slightly closer to zero than those for in-situ-UW. This matches the findings of too dry an atmosphere from the radiosonde readings; the in-situ-UW simulated atmosphere is more transparent in this spectral range and so permits more thermal radiation to escape to space from the (near-)surface than is observed. A slight positive bias in the residuals in scene 6 could also point to issues with the surface specification. residuals again have a similar structure, with positive peaks around $\sim$480 cm^{-1} and negative values towards the higher-energy end of the band. Some scatter is also clear; more than half of channels in the band lie beyond the uncertainty range in scene 5, while agreement is slightly stronger in scene 6. This is despite the scene surface heterogeneity being higher in scene 6. In the FIR-2 band (170–340 cm^{-1}), the number of points lying outside of the uncertainty bounds suggests that the total radiance uncertainty of the instrument is underestimated at present; the instrument noise makes further quantitative deductions difficult.

5.1 Use of GOES ABI surface temperature

The findings of a consistent positive bias of simulations relative to PREFIRE observations in the infrared window region prompts a re-evaluation of the simulated surface properties. Surface emissivities in the mid-infrared are sufficiently well-constrained and constant across surface types to preclude this being the sole cause of the residuals seen, so we explore modifications of the emitting skin temperature.

To find an alternative source of this T_{sfc}, we turn to observations from geostationary platforms. Specifically, from the GOES-16 satellite we take the Advanced Baseline Imager's (ABI) full-disk land surface temperature retrieval (ABI-L2-LST). This is sampled at 21:00 UTC, just seven minutes after the PREFIRE overpass, and has a 10 resolution at nadir. For each PREFIRE scene, we take an average of the ABI retrieved land surface temperature readings within the TIRS FOV polygons weighted by area and overlap fraction. The resulting temperatures (256.8 ± 0.7 and 256.7 ± 0.6 for scenes 5 and 6 respectively) then replace the ERA5 T_{sfc} in otherwise identical simulations.

The resulting residuals from the simulations with modified T_{sfc} are shown as dashed lines in Fig. 6. In the MIR-2 band, the inclusion of the ABI T_{sfc} significantly improves the residuals, with most channels' residuals now lying within the uncertainty bands. In the FIR-1 band an improvement is clear for both simulations in scene 6, while any improvement in scene 5 is marginal.

6 Discussion

Given the excellent agreement of the ~~ERA5-DW~~ profile C simulation with observations by the FINESSE instrument, we infer that this profile represents a robust knowledge of the overlying atmosphere. The corresponding simulation for PREFIRE ~~, when using the observed ABI T_{sfc},~~ also lies close to the observations, but ~~slightly~~ more spectral points lie outside the uncertainty limits than would be expected, especially in the FIR-2 band. We believe that, with all other uncertainties accounted for, these anomalous residuals are ~~mostly~~ primarily a result of ~~instrument effects~~issues with the TIRS instrument. In the MIR-2 and FIR-1 bands, where residuals show a similar pattern for the two scenes, the similarity hints at a common cause warranting further investigation, such as calibration error remaining even after the radiance bias correction. In the FIR-2 band, the principal cause is likely detector noise, which is perhaps underestimated at present. We note that the current PREFIRE L1B products mark all FIR-2 band channels with a flag indicating the quality is unknown and that there may be calibration biases. It is worth highlighting that for both FINESSE and PREFIRE, the largest uncertainties are found in the far-infrared.

We preface this discussion by highlighting the limitations of investigating just one case. Combining results from many overpasses would strengthen our validation and provide more rigorous quantitative conclusions, especially given that there is a broad range of PREFIRE observation conditions to test: observations from different sensors in the cross-track array, observations from Satellite 2, and different in-orbit environments to which there may be some sensitivity (daytime/nighttime causing thermal effects in the satellite bus). However, by focusing on a single case we have been able to optimise the atmospheric profile and consider a range of uncertainties in the closure tests. We hope that the rigorous methodology of this study can be employed to strengthen future longer-term monitoring and validation experiments.

The detailed analysis of uncertainties in Sect. 3 allows us to identify the main sources of uncertainty in the experiment. For FINESSE, specification of water vapour profiles is a large source of uncertainty in both simulations, especially in the FIR. ~~This is slightly larger in the in-situ case, where we have treated systematic errors in the radiosonde measurements as fully vertically correlated. The residuals shown in the in-situ-DW case, however,~~ Furthermore, the residuals from the profile A simulation lead us to question the veracity of the radiosonde measurements. ~~Several studies have noted dry biases in radiosonde measurements, particularly in dry conditions (Vömel et al., 2007; Rowe et al., 2008; Miloshevich et al., 2009; Dzambo et al., 2016).~~ Our results suggest a ~~similar dry bias for~~ dry bias in the iMet-4 radiosonde ~~as~~ measurements used in the WHAFFFERS campaign~~, which has not yet been thoroughly investigated.~~

~~Given the radiosonde residual bias in the FIR and the good performance of the ERA5-DW profile, we investigate a bias correction method~~. This is a feature that other authors have noted in measurements by other radiosonde models, particularly in dry conditions (Vömel et al., 2007; Rowe et al., 2008; Miloshevich et al., 2009; Dzambo et al., 2016). The total moisture content of the column measured by radiosondes over the entire WHAFFFERS campaign was calculated and compared to values calculated from ERA5 following each radiosonde track (as in Sect. 3.2). Of the ten launches without issue, seven featured very low column water vapour <3 mm. Across these seven cases, the radiosonde measurements exhibit a consistent dry bias of about 9 % relative to ERA5 (i.e. $CWV_{\mathrm{sonde}} \approx 0.91 \times CWV_{\mathrm{ERA5}}$). ~~Remedying this bias by a scalar adjustment of the radiosonde-measured water column and re-running the experiment much improves agreement with the bias-adjusted~~

in-situ-DW case, even outperforming the ERA5-DW case in the FIR (not shown). We thus conclude that it is likely that the radiosonde has a dry humidity bias in these conditions. However, we also cannot rule out the possibility that this radiosonde bias is caused by campaign-specific errors in the launch process.

We recommend that for closure experiments, radiosondes be used in tandem with either a trusted bias correction algorithm or an auxiliary source of information. This information could come from reanalysis, as in our brief investigation, but ideally it would be from collocated measurements, such as retrievals from microwave sensors. We argue further that passive remote sensing in spectral regions different to those measured by the closure-targeting instrument is crucial to ensure strengthens results by ensuring independence of observations from simulations.

Uncertainties in the FIR spectroscopy of water vapour also have a sizeable impact on modelling FINESSE radiances . radiances at high spectral resolution, such as for FINESSE. We note that the uncertainties here derive from the rather inexact uncertainty codes of the HITRAN database, and we encourage the spectroscopy community to publish experimental uncertainty information, including spectral covariance, for their measurements of spectral lines, and to ensure that these are uncertainties are documented in spectroscopic databases. Further closure or laboratory studies may also be able to address thisreduce the magnitude of these uncertainties.

The appearance of some residuals beyond uncertainty for FINESSE between 390–400 cm^{-1} in both for all simulations was investigated by comparing the simulated and measured radiances to 160 spectra acquired over a 60 minute window, each one an average of 20 scans. The many individual spectra showed a large spread in which the residual signal was not an outlier (not shown). The fact that residuals lie beyond the uncertainty limits could indicate that the FINESSE NESR is under-reported in this region, and/or that the extension of FINESSE to 380 cm^{-1} requires further validation.

Finally for FINESSE, characterising the air temperature very near the instrument is key. There are some significant residuals for wavenumbers with strong sensitivity to the surface layers, especially in the emission features (c. 600–750). Readings from FINESSE's auxiliary temperature sensor were anomalous in this field campaign and so not used; ensuring valid measurements from this sensor could enhance the robustness of future closure tests with FINESSE.

PREFIRE closure diagnosis in the FIR, particularly in the FIR-2 band, is largely hindered by instrument noise. Further evaluation of persistent biases could be possible using substantial averaging. In similar conditions to this study, this noise would no longer be a dominant uncertainty source in the FIR-1 band after averaging over 10 spectra, or 150 spectra in the FIR-2 band, for PREFIRE satellite 1. Satellite 2 has a higher instrument noise which would require approximately twice as many spectra. A study using a set-up like ours employing an averaging approach would hence require a long-term ground-based spectrometer data record (possibly over 12 months to build up the clear sky statistics required, though latitude dependent), and may not be able to use radiosonde data for the quantity of overflights needed. Uncertainty in the radiosonde water vapour specification is comparable to instrument noise around 350–500 cm^{-1} and would become a leading uncertainty source with more averaging of spectra, reinforcing the need for precise water vapour measurements in FIR closure studies.

In the MIR, the dominant uncertainty for PREFIRE is due to the temperature of the underlying surface, with its emissivity also playing an important role. The importance of While we are able to estimate the surface temperature in this setup is further reinforced by the finding of a drastic improvement, in this instance, of taking this figure from the GOES-ABI rather than

ERA5. Due using a geostationary sensor in this case, the emissivity is much harder to quantify and we are reliant on a single theoretical model, namely that by Huang et al. (2016). PREFIRE will provide estimates of surface emissivity in polar regions, but we highlight the potential for more modelling and observational efforts to further constrain spectral surface emissivity, and its uncertainty, in the FIR. In practice for future campaigns, due to the large area of the measured swath, a ground-based temperature or emissivity measurement would likely only be representative for a very homogeneous surface. Another A possibility is to remotely sense the surface temperature or emissivity with a drone-mounted instrument in the region around the ground station; this platform could then additionally sample the nearby variation in the humidity field. Radiances observed by a low-flying aircraft could also be used to retrieve surface temperature and emissivity separately, as demonstrated by Bellisario et al. (2017).

There is also further opportunity for satellite-to-satellite validation of PREFIRE, in the MIR spectral region, using geostationary satellites. They offer coverage over a large swath with much shorter repeat times than polar-orbiting missions. The Infrared Sounder on the Meteosat Third Generation (MTG-IRS) will provide spectrally resolved mid-infrared radiances from a geostationary platform. This could yield plentiful opportunities to perform radiance comparisons under a range of conditions for the PREFIRE MIR channels. Here a key issue to resolve would be the impact of viewing geometry.

Finally, we note that the simulations performed for this study have already proven useful in validating improvements in the second release of the PREFIRE L1B radiance product (though direct comparison of simulations to the first release is not shown in this paper) , and can continue to be used as a benchmark for future revisions.

7 Conclusions

In this paper, we have performed a 'ground-to-space' radiative closure study using the FINESSE instrument and an overpass of the PREFIRE satellite 1. To our knowledge, this is the first attempt at this type of experiment in the far-infrared. Thorough consideration of the various sources of uncertainty confirmed the validity of this approach and illustrated the main challenges in this experiment.

The ground-based FINESSE instrument demonstrated excellent closure , in particular when simulations used atmospheric data from good radiance closure using a profile based principally on data from a collocated iMet-4 radiosonde launch. However, notable deficiencies were apparent, spectrally manifested across the 15 µm CO_2 band (∼600–750 cm^{-1}) and in the far-infrared from 400–600 cm^{-1}. We could reconcile the former bias with a small (<1 K) shift in the whole temperature profile. The latter discrepancy was resolved by scaling the radiosonde-measured atmospheric water vapour to match the higher total column water vapour found in the collocated profile from ERA5reanalysis. Simulations based on in situ data did not agree as well with the FINESSE observations. This is a contrasting result to that found with FINESSE by Mosselmans et al. (2026), but may reflect the use of a different radiosonde brand in our study. The radiance results, and . Applying both the temperature and water vapour scaling led to excellent agreement between the resulting downwelling radiance simulation and FINESSE measurements, providing an optimised profile for input to our upwelling simulations for PREFIRE.

We noted that additional comparisons between ERA5 profiles and ~~radiosonde launches~~ coincident iMet-4 radiosonde launches made throughout the WHAFFFERS campaign ~~, led us to conclude that there is likely a dry bias in humidity measurements from~~ revealed a persistent offset between humidity in the reanalysis and in the measurements. We concluded that the iMet-4 radiosonde ~~in the~~ suffers from a persistent dry bias which is of the order ∼9 % (relative to reanalysis) under the very dry conditions ~~of~~ experienced during the campaign.

The largest source of uncertainty in the comparison between simulated and observed FINESSE radiances was in the specification of atmospheric water vapour profile, followed by the spectroscopy of water vapour. Many other authors note that precisely determining water vapour spectroscopy from field studies is limited by uncertainties in atmospheric water vapour content, and so we encourage further laboratory study and for future field studies targeting the region to be designed with accurate, precise, and independent determination of ~~water vapour~~ atmospheric humidity at their core. These techniques will also help to calibrate and validate observations from the upcoming Far-infrared Outgoing Radiation Understanding and Monitoring (FORUM) satellite mission, scheduled to launch in 2028 (Palchetti et al., 2020).

The agreement of PREFIRE observations of upwelling radiances at the top-of-the-atmosphere with simulations using the optimised profile varied by spectral region. In the mid-infrared~~and FIR dirty window~~, the agreement ~~is~~ was only slightly weaker than obtained for the downwelling FINESSE measurements, ~~though~~ while in the FIR dirty window (350–630 cm^{-1}) agreement was weaker still, with more scatter in the PREFIRE residual points~~are more scattered~~. In the furthest infrared band (185–330 cm^{-1}) agreement was ~~somewhat~~ poorer, largely due to a high radiometric noise in the PREFIRE TIRS instrument which may be underestimated at present. ~~We also noted that inaccurate specification of water vapour by the radiosonde, diagnosed by FINESSE, degraded the PREFIRE residuals in the FIR dirty window, reinforcing the importance of water vapour profiling for these experiments. In these dry conditions , the infrared window and the~~ In the principal infrared window, uncertainty in our results was dominated by specification of surface temperature and emissivity. Under the dry conditions observed here, the FIR dirty window ~~are both~~ is more sensitive to the surface ~~, and so uncertainty in our results was dominated by specification of surface temperature and emissivity in these spectral regions. We found that the use of independent satellite-observed surface temperature was able to remedy a bias in that from ERA5. However, it appears there remain some small systematic errors . Rigorous~~ at higher wavenumbers and to the atmospheric water vapour at lower wavenumbers, so both of these factors are key uncertainty sources in this spectral region. We discussed potential options for reducing the surface uncertainty, including the use of other field or satellite measurements. We found some systematic errors in the PREFIRE residuals beyond the uncertainties considered; rigorous quantification of these errors will require further targeted comparisons over a longer time period and a wider range of conditions. We note that the approach developed here, and the database of simulated radiances with associated uncertainties, will be useful for validating further efforts by the PREFIRE team to correct biases in the measured radiances. ~~We discussed potential options for reducing the surface uncertainty, including the use of other field or satellite measurements.~~

PREFIRE, and the upcoming FORUM mission, open a new measurement window from space. They are designed to exploit the information content within the far-infrared to provide new insights into water vapour distributions, the radiative effects of clouds and, where conditions permit, surface properties. However, the community must be prepared with the right set of

experimental designs and auxiliary measurement capabilities to comprehensively validate the new observations and hence maximise their scientific impact. Our study provides a stepping stone towards this goal.

Data availability. At time of submission, measurement data used in this study from the WHAFFFERS campaign are not yet available in an open archive, but can be accessed upon request to the authors.

Author contributions. BP and HB conceived the study. BP carried out the investigation and wrote the first draft of the manuscript, with supervision from HB and RH. JM, SM, SP, LW, YH, and BR-B took field measurements on the WHAFFFERS campaign. TL provided PREFIRE expertise and data curation. SM, SP, LW, and BR-B provided input to the radiative transfer modelling methodology. HO, DS, HB, and YH assisted with funding acquisition and project administration for the WHAFFFERS campaign. All authors assisted with editing the manuscript.

Competing interests. The authors declare that they have no conflict of interest.

Acknowledgements. The deployment of FINESSE on the WHAFFFERS campaign was supported by the European Space Agency (ESA) with grant number 4000137153/22/NL/IA. BP, SM, and SP were funded by the UK Natural Environment Research Council (NERC) via the SSCP DTP, grant number NE/S007415/1. HB and JM were supported by NERC under grant no. NE/Y006216/1. Field data were recorded at the Gault Nature Reserve of McGill University. For their contributions to the operation of the WHAFFFERS campaign we thank Lei Liu, Ruogu He, Mathieu Noreau, Eve Bigras, Veronique Meunier, and Calin Giurgiu from McGill University, and Jonathan Gero from University of Wisconsin-Madison. We would like to thank Aronne Merrelli, Nathaniel Miller, and Tim Michaels on the PREFIRE team for their assistance with data access and manuscript review.

References

Agustí-Panareda, A., Diamantakis, M., Massart, S., Chevallier, F., Muñoz-Sabater, J., Barré, J., Curcoll, R., Engelen, R., Langerock, B., Law, R. M., Loh, Z., Morguí, J. A., Parrington, M., Peuch, V.-H., Ramonet, M., Roehl, C., Vermeulen, A. T., Warneke, T., and Wunch, D.: Modelling CO2 weather – why horizontal resolution matters, Atmospheric Chemistry and Physics, 19, 7347–7376, https://doi.org/10.5194/acp-19-7347-2019, 2019.

Bantges, R. J., Brindley, H. E., Murray, J. E., Last, A. E., Russell, J. E., Fox, C., Fox, S., Harlow, C., O'Shea, S. J., Bower, K. N., Baum, B. A., Yang, P., Oetjen, H., and Pickering, J. C.: A test of the ability of current bulk optical models to represent the radiative properties of cirrus cloud across the mid- and far-infrared, Atmospheric Chemistry and Physics, 20, 12 889–12 903, https://doi.org/10.5194/acp-20-12889-2020, 2020.

Baran, A. J.: The impact of cirrus microphysical and macrophysical properties on upwelling far-infrared spectra, Quarterly Journal of the Royal Meteorological Society, 133, 1425–1437, https://doi.org/10.1002/qj.132, _eprint: https://rmets.onlinelibrary.wiley.com/doi/pdf/10.1002/qj.132, 2007.

Bellisario, C., Brindley, H. E., Murray, J. E., Last, A., Pickering, J., Harlow, R. C., Fox, S., Fox, C., Newman, S. M., Smith, M., Anderson, D., Huang, X., and Chen, X.: Retrievals of the Far Infrared Surface Emissivity Over the Greenland Plateau Using the Tropospheric Airborne Fourier Transform Spectrometer (TAFTS), Journal of Geophysical Research: Atmospheres, 122, https://doi.org/10.1002/2017JD027328, 2017.

Belotti, C., Barbara, F., Barucci, M., Bianchini, G., D'Amato, F., Del Bianco, S., Di Natale, G., Gai, M., Montori, A., Pratesi, F., Rettinger, M., Rolf, C., Sussmann, R., Trickl, T., Viciani, S., Vogelmann, H., and Palchetti, L.: The Far-Infrared Radiation Mobile Observation System (FIRMOS) for spectral characterization of the atmospheric emission, Atmospheric Measurement Techniques, 16, 2511–2529, https://doi.org/10.5194/amt-16-2511-2023, 2023.

Brindley, H. E. and Harries, J. E.: The impact of far i.r. absorption on clear sky greenhouse forcing: sensitivity studies at high spectral resolution, Journal of Quantitative Spectroscopy and Radiative Transfer, 60, 151–180, https://doi.org/10.1016/S0022-4073(97)00152-0, 1998.

Bullister, J. L. and Warner, M. J.: Atmospheric Histories (1765-2022) for CFC-11, CFC-12, CFC-113, CCl4, SF6 and N2O (NCEI Accession 0164584), https://doi.org/10.3334/CDIAC/OTG.CFC_ATM_HIST_2015, 2017.

Chen, X., Huang, X., and Flanner, M. G.: Sensitivity of modeled far-IR radiation budgets in polar continents to treatments of snow surface and ice cloud radiative properties, Geophysical Research Letters, 41, 6530–6537, https://doi.org/10.1002/2014GL061216, 2014.

Clough, S. A., Shephard, M. W., Mlawer, E. J., Delamere, J. S., Iacono, M. J., Cady-Pereira, K., Boukabara, S., and Brown, P. D.: Atmospheric radiative transfer modeling: a summary of the AER codes, Journal of Quantitative Spectroscopy and Radiative Transfer, 91, 233–244, https://doi.org/10.1016/j.jqsrt.2004.05.058, 2005.

Delamere, J. S., Clough, S. A., Payne, V. H., Mlawer, E. J., Turner, D. D., and Gamache, R. R.: A far-infrared radiative closure study in the Arctic: Application to water vapor, Journal of Geophysical Research: Atmospheres, 115, 2009JD012 968, https://doi.org/10.1029/2009JD012968, 2010.

Di Natale, G., Brindley, H., Warwick, L., Panditharatne, S., Yang, P., David, R. O., Carlsen, T., Vâjâiac, S. N., Vlad, A., Ghemuleț, S., Bantges, R., Foth, A., Flügge, M., Lyngra, R., Oetjen, H., Schuettemeyer, D., Palchetti, L., and Murray, J.: Achieving consistency between in-situ and remotely sensed optical and microphysical properties of Arctic cirrus: the impact of far-infrared radiances, Atmospheric Chemistry and Physics, 26, 1373–1394, https://doi.org/10.5194/acp-26-1373-2026, 2026.

Drouin, B., Merrelli, A., and Michaels, T.: PREFIRE Spectral Response Function data (SRFs): v13, https://doi.org/10.5281/ZENODO.16638853, 2025a.

Drouin, B. J., L'Ecuyer, T., Padmanabhan, S., Foote, M., Bendig, R., Calcutt, S., Hawkins, G., Herzog, H., Hochberg, E., Kenyon, M., Mariani, G., Martinez, D. A., McGuire, J., Mckinley, I., Merrelli, A., Nemchick, D., Raouf, N., Spiers, G., and Wilson, D.: Thermal Infrared Spectrometers for the Polar Radiant Energy in the Far-Infrared Experiment (PREFIRE), Earth and Space Science, 12, e2024EA003 711, https://doi.org/10.1029/2024EA003711, 2025b.

Dzambo, A. M., Turner, D. D., and Mlawer, E. J.: Evaluation of two Vaisala RS92 radiosonde solar radiative dry bias correction algorithms, Atmospheric Measurement Techniques, 9, 1613–1626, https://doi.org/10.5194/amt-9-1613-2016, 2016.

Feldman, D. R., Liou, K. N., Shia, R. L., and Yung, Y. L.: On the information content of the thermal infrared cooling rate profile from satellite instrument measurements, Journal of Geophysical Research: Atmospheres, 113, 2007JD009 041, https://doi.org/10.1029/2007JD009041, 2008.

Fischer, L., Craig, G. C., and Kiemle, C.: Horizontal structure function and vertical correlation analysis of mesoscale water vapor variability observed by airborne lidar, Journal of Geophysical Research: Atmospheres, 118, 7579–7590, https://doi.org/10.1002/jgrd.50588, 2013.

Flores, F., Rondanelli, R., Díaz, M., Querel, R., Mundnich, K., Herrera, L. A., Pola, D., and Carricajo, T.: The Life Cycle of a Radiosonde, Bulletin of the American Meteorological Society, 94, 187–198, https://doi.org/10.1175/BAMS-D-11-00163.1, 2013.

Ghysels, M., Durry, G., Amarouche, N., Hurst, D., Hall, E., Xiong, K., Dupont, J.-C., Samake, J.-C., Frérot, F., Bejjani, R., and Riviere, E. D.: Pico-Light H_2 O: intercomparison of in situ water vapour measurements during the AsA 2022 campaign, Atmospheric Measurement Techniques, 17, 3495–3513, https://doi.org/10.5194/amt-17-3495-2024, 2024.

GOES-R Algorithm Working Group and GOES-R Series Program: NOAA GOES-R Series Advanced Baseline Imager (ABI) Level 2 Land Surface Temperature (LST), https://doi.org/10.7289/V52R3PZ8, 2018.

Han, Y., Revercomb, H., Cromp, M., Gu, D., Johnson, D., Mooney, D., Scott, D., Strow, L., Bingham, G., Borg, L., Chen, Y., DeSlover, D., Esplin, M., Hagan, D., Jin, X., Knuteson, R., Motteler, H., Predina, J., Suwinski, L., Taylor, J., Tobin, D., Tremblay, D., Wang, C., Wang, L., Wang, L., and Zavyalov, V.: Suomi NPP CrIS measurements, sensor data record algorithm, calibration and validation activities, and record data quality, Journal of Geophysical Research: Atmospheres, 118, https://doi.org/10.1002/2013JD020344, 2013.

Hanel, R. A., Schlachman, B., Rogers, D., and Vanous, D.: Nimbus 4 Michelson Interferometer, Applied Optics, 10, 1376, https://doi.org/10.1364/AO.10.001376, 1971.

Harries, J., Carli, B., Rizzi, R., Serio, C., Mlynczak, M., Palchetti, L., Maestri, T., Brindley, H., and Masiello, G.: The Far-infrared Earth, Reviews of Geophysics, 46, https://doi.org/https://doi.org/10.1029/2007RG000233, _eprint: https://agupubs.onlinelibrary.wiley.com/doi/pdf/10.1029/2007RG000233, 2008.

Hersbach, H., Bell, B., Berrisford, P., Hirahara, S., Horányi, A., Muñoz-Sabater, J., Nicolas, J., Peubey, C., Radu, R., Schepers, D., Simmons, A., Soci, C., Abdalla, S., Abellan, X., Balsamo, G., Bechtold, P., Biavati, G., Bidlot, J., Bonavita, M., De Chiara, G., Dahlgren, P., Dee, D., Diamantakis, M., Dragani, R., Flemming, J., Forbes, R., Fuentes, M., Geer, A., Haimberger, L., Healy, S., Hogan, R. J., Hólm, E., Janisková, M., Keeley, S., Laloyaux, P., Lopez, P., Lupu, C., Radnoti, G., de Rosnay, P., Rozum, I., Vamborg, F., Villaume, S., and Thépaut, J.-N.: The ERA5 global reanalysis, Quarterly Journal of the Royal Meteorological Society, 146, 1999–2049, https://doi.org/https://doi.org/10.1002/qj.3803, _eprint: https://rmets.onlinelibrary.wiley.com/doi/pdf/10.1002/qj.3803, 2020.

Hilton, F., Armante, R., August, T., Barnet, C., Bouchard, A., Camy-Peyret, C., Capelle, V., Clarisse, L., Clerbaux, C., Coheur, P.-F., Collard, A., Crevoisier, C., Dufour, G., Edwards, D., Faijan, F., Fourrié, N., Gambacorta, A., Goldberg, M., Guidard, V., Hurtmans, D., Illingworth, S., Jacquinet-Husson, N., Kerzenmacher, T., Klaes, D., Lavanant, L., Masiello, G., Matricardi, M., McNally, A., Newman, S., Pavelin, E.,

Payan, S., Péquignot, E., Peyridieu, S., Phulpin, T., Remedios, J., Schlüssel, P., Serio, C., Strow, L., Stubenrauch, C., Taylor, J., Tobin, D., Wolf, W., and Zhou, D.: Hyperspectral Earth Observation from IASI: Five Years of Accomplishments, Bulletin of the American Meteorological Society, 93, 347–370, https://doi.org/10.1175/BAMS-D-11-00027.1, 2012.

Hogan, R. J. and Matricardi, M.: Evaluating and improving the treatment of gases in radiation schemes: the Correlated K-Distribution Model Intercomparison Project (CKDMIP), Geoscientific Model Development, 13, 6501–6521, https://doi.org/10.5194/gmd-13-6501-2020, 2020.

Hokanson Wagner, E., Drouin, B., Michaels, T., and Merrelli, A.: PREFIRE Data User Guide: Level 1B Radiance (1B-RAD), Tech. rep., https://asdc.larc.nasa.gov/documents/prefire/guide/PREFIRE_Data_User_Guide_1B-RAD_R01-20250430.pdf, version R01, 2025.

Huang, X., Chen, X., Zhou, D. K., and Liu, X.: An Observationally Based Global Band-by-Band Surface Emissivity Dataset for Climate and Weather Simulations, Journal of the Atmospheric Sciences, 73, 3541 – 3555, https://doi.org/10.1175/JAS-D-15-0355.1, place: Boston MA, USA, 2016.

Huang, X., Chen, X., Flanner, M., Yang, P., Feldman, D., and Kuo, C.: Improved Representation of Surface Spectral Emissivity in a Global Climate Model and Its Impact on Simulated Climate, Journal of Climate, 31, 3711–3727, https://doi.org/10.1175/JCLI-D-17-0125.1, 2018.

Hurst, D. F., Hall, E. G., Jordan, A. F., Miloshevich, L. M., Whiteman, D. N., Leblanc, T., Walsh, D., Vömel, H., and Oltmans, S. J.: Comparisons of temperature, pressure and humidity measurements by balloon-borne radiosondes and frost point hygrometers during MOHAVE-2009, Atmospheric Measurement Techniques, 4, 2777–2793, https://doi.org/10.5194/amt-4-2777-2011, 2011.

InterMet Systems: iMet-4 Radiosonde Technical Data Sheet, Tech. rep., InterMet Systems, Grand Rapids, MI, USA, https://www.intermetsystems.com/wp-content/uploads/2022/01/202084-12_iMet-4_Technical_Data_Sheet.pdf, 2022.

Kempe, V., Oertel, D., Schuster, R., Becker-Ross, H., and Jahn, H.: Absolute IR-spectra from the measurement of Fourier-spectrometers aboard Meteor 25 and 28, Acta Astronautica, 7, 1403–1416, https://doi.org/10.1016/0094-5765(80)90015-6, 1980.

Liu, L., Bliankinshtein, N., Huang, Y., Gyakum, J. R., Gabriel, P. M., Xu, S., and Wolde, M.: Radiative closure tests of collocated hyperspectral microwave and infrared radiometers, Atmospheric Measurement Techniques, 17, 2219–2233, https://doi.org/10.5194/amt-17-2219-2024, 2024.

Liu, X., Smith, W. L., Zhou, D. K., and Larar, A.: Principal component-based radiative transfer model for hyperspectral sensors: theoretical concept, Applied Optics, 45, 201, https://doi.org/10.1364/AO.45.000201, 2006.

L'Ecuyer, T. S., Drouin, B. J., Anheuser, J., Grames, M., Henderson, D. S., Huang, X., Kahn, B. H., Kay, J. E., Lim, B. H., Mateling, M., Merrelli, A., Miller, N. B., Padmanabhan, S., Peterson, C., Schlegel, N.-J., White, M. L., and Xie, Y.: The Polar Radiant Energy in the Far Infrared Experiment: A New Perspective on Polar Longwave Energy Exchanges, Bulletin of the American Meteorological Society, 102, E1431 – E1449, https://doi.org/10.1175/BAMS-D-20-0155.1, place: Boston MA, USA, 2021.

Maestri, T., Rizzi, R., Tosi, E., Veglio, P., Palchetti, L., Bianchini, G., Di Girolamo, P., Masiello, G., Serio, C., and Summa, D.: Analysis of cirrus cloud spectral signatures in the far infrared, Journal of Quantitative Spectroscopy and Radiative Transfer, 141, 49–64, https://doi.org/10.1016/j.jqsrt.2014.02.030, 2014.

Mariani, Z., Strong, K., Wolff, M., Rowe, P., Walden, V., Fogal, P. F., Duck, T., Lesins, G., Turner, D. S., Cox, C., Eloranta, E., Drummond, J. R., Roy, C., Turner, D. D., Hudak, D., and Lindenmaier, I. A.: Infrared measurements in the Arctic using two Atmospheric Emitted Radiance Interferometers, Atmospheric Measurement Techniques, 5, 329–344, https://doi.org/10.5194/amt-5-329-2012, 2012.

Mattingly, K., Hokanson Wagner, E., Michaels, T., and Merrelli, A.: PREFIRE Data User Guide Auxiliary Meteorology (AUX-MET), Tech. rep., https://asdc.larc.nasa.gov/documents/prefire/guide/PREFIRE_Data_User_Guide_AUX-MET_R01.pdf, version R01, 2025.

Miloshevich, L. M., Vömel, H., Whiteman, D. N., and Leblanc, T.: Accuracy assessment and correction of Vaisala RS92 radiosonde water vapor measurements, Journal of Geophysical Research: Atmospheres, 114, 2008JD011 565, https://doi.org/10.1029/2008JD011565, 2009.

Mlawer, E. J., Turner, D. D., Paine, S. N., Palchetti, L., Bianchini, G., Payne, V. H., Cady-Pereira, K. E., Pernak, R. L., Alvarado, M. J., Gombos, D., Delamere, J. S., Mlynczak, M. G., and Mast, J. C.: Analysis of Water Vapor Absorption in the Far-Infrared and Submillimeter Regions Using Surface Radiometric Measurements From Extremely Dry Locations, Journal of Geophysical Research: Atmospheres, 124, 8134–8160, https://doi.org/10.1029/2018JD029508, 2019.

Mlawer, E. J., Cady-Pereira, K. E., Mascio, J., and Gordon, I. E.: The inclusion of the MT_CKD water vapor continuum model in the HITRAN molecular spectroscopic database, Journal of Quantitative Spectroscopy and Radiative Transfer, 306, 108 645, https://doi.org/https://doi.org/10.1016/j.jqsrt.2023.108645, 2023.

Mosselmans, S., Elizabeth Brindley, H., Cox, C., Gryspeerdt, E., Murray, J., Panditharatne, S., Warwick, L., Schuettemeyer, D., Oetjen, H., Carlsen, T., Foth, A., and David, R.: Exploring Clear-Sky Longwave Radiative Closure in the Arctic: A Downwelling Case Study, Atmospheric Science Letters, 27, e70 000, https://doi.org/10.1002/asl.70000, 2026.

Murray, J. E., Brindley, H. E., Fox, S., Bellisario, C., Pickering, J. C., Fox, C., Harlow, C., Smith, M., Anderson, D., Huang, X., Chen, X., Last, A., and Bantges, R.: Retrievals of High-Latitude Surface Emissivity Across the Infrared From High-Altitude Aircraft Flights, Journal of Geophysical Research: Atmospheres, 125, e2020JD033 672, https://doi.org/10.1029/2020JD033672, 2020.

Murray, J. E., Warwick, L., Brindley, H., Last, A., Quigley, P., Rochester, A., Dewar, A., and Cummins, D.: The Far-INfrarEd Spectrometer for Surface Emissivity (FINESSE) – Part 1: Instrument description and level 1 radiances, Atmospheric Measurement Techniques, 17, 4757–4775, https://doi.org/10.5194/amt-17-4757-2024, 2024.

NOAA: Global Monitoring Laboratory: Carbon Cycle Greenhouse Gases, https://gml.noaa.gov/ccgg/data/.

Oreopoulos, L., Mlawer, E., Delamere, J., Shippert, T., Cole, J., Fomin, B., Iacono, M., Jin, Z., Li, J., Manners, J., Räisänen, P., Rose, F., Zhang, Y., Wilson, M. J., and Rossow, W. B.: The Continual Intercomparison of Radiation Codes: Results from Phase I, Journal of Geophysical Research: Atmospheres, 117, 2011JD016 821, https://doi.org/10.1029/2011JD016821, 2012.

Palchetti, L., Brindley, H., Bantges, R., Buehler, S. A., Camy-Peyret, C., Carli, B., Cortesi, U., Del Bianco, S., Di Natale, G., Dinelli, B. M., Feldman, D., Huang, X. L., C.-Labonnote, L., Libois, Q., Maestri, T., Mlynczak, M. G., Murray, J. E., Oetjen, H., Ridolfi, M., Riese, M., Russell, J., Saunders, R., and Serio, C.: FORUM: Unique Far-Infrared Satellite Observations to Better Understand How Earth Radiates Energy to Space, Bulletin of the American Meteorological Society, 101, E2030–E2046, https://doi.org/10.1175/BAMS-D-19-0322.1, 2020.

Panditharatne, S., Cox, C., Song, R., Siddans, R., Bantges, R., Murray, J., Fox, S., Fox, C., and Brindley, H.: Exploiting airborne far-infrared measurements to optimise an ice cloud retrieval, Atmospheric Chemistry and Physics, 25, 9981–9998, https://doi.org/10.5194/acp-25-9981-2025, 2025.

Ridolfi, M., Tirelli, C., Ceccherini, S., Belotti, C., Cortesi, U., and Palchetti, L.: Synergistic retrieval and complete data fusion methods applied to simulated FORUM and IASI-NG measurements, Atmospheric Measurement Techniques, 15, 6723–6737, https://doi.org/10.5194/amt-15-6723-2022, 2022.

Rodgers, C. D.: Inverse Methods for Atmospheric Sounding: Theory and Practice, vol. 2 of *Series on Atmospheric, Oceanic and Planetary Physics*, WORLD SCIENTIFIC, ISBN 978-981-02-2740-1 978-981-281-371-8, https://doi.org/10.1142/3171, 2000.

Rowe, P. M., Miloshevich, L. M., Turner, D. D., and Walden, V. P.: Dry Bias in Vaisala RS90 Radiosonde Humidity Profiles over Antarctica, Journal of Atmospheric and Oceanic Technology, 25, 1529–1541, https://doi.org/10.1175/2008JTECHA1009.1, 2008.

Sinha, A. and Harries, J. E.: Water vapour and greenhouse trapping: The role of far infrared absorption, Geophysical Research Letters, 22, 2147–2150, https://doi.org/10.1029/95GL01891, 1995.

Sussmann, R., Reichert, A., and Rettinger, M.: The Zugspitze radiative closure experiment for quantifying water vaporabsorption over the terrestrial and solar infrared –Part 1: Setup, uncertainty analysis, and assessment of far-infrared watervapor continuum, Atmospheric Chemistry and Physics, 16, 11 649–11 669, https://doi.org/10.5194/acp-16-11649-2016, 2016.

Turner, D. D., Merrelli, A., Vimont, D., and Mlawer, E. J.: Impact of modifying the longwave water vapor continuum absorption model on community Earth system model simulations, Journal of Geophysical Research: Atmospheres, 117, 2011JD016 440, https://doi.org/10.1029/2011JD016440, 2012.

Vaisala: HMP155 User Guide, Tech. rep., Vaisala, Vantaa, Finland, https://docs.vaisala.com/r/M210912EN-J/en-US, 2025.

Vömel, H., Selkirk, H., Miloshevich, L., Valverde-Canossa, J., Valdés, J., Kyrö, E., Kivi, R., Stolz, W., Peng, G., and Diaz, J. A.: Radiation Dry Bias of the Vaisala RS92 Humidity Sensor, Journal of Atmospheric and Oceanic Technology, 24, 953–963, https://doi.org/10.1175/JTECH2019.1, 2007.

Wang, S., Ren, T., Yang, P., Saito, M., and Brindley, H. E.: Improved Temperature-Dependent Ice Refractive Index Compilation in the Far-Infrared Spectrum, Geophysical Research Letters, 51, e2024GL110 176, https://doi.org/10.1029/2024GL110176, _eprint: https://agupubs.onlinelibrary.wiley.com/doi/pdf/10.1029/2024GL110176, 2024.

Warwick, L., Brindley, H., Di Roma, A., Fox, S., Havemann, S., Murray, J., Oetjen, H., Price, H. C., Schüttemeyer, D., Sgheri, L., and Tiddeman, D. A.: Retrieval of Tropospheric Water Vapor From Airborne Far-Infrared Measurements: A Case Study, Journal of Geophysical Research: Atmospheres, 127, e2020JD034 229, https://doi.org/10.1029/2020JD034229, 2022.

Warwick, L., Murray, J. E., and Brindley, H.: The Far-INfrarEd Spectrometer for Surface Emissivity (FINESSE) – Part 2: First measurements of the emissivity of water in the far-infrared, Atmospheric Measurement Techniques, 17, 4777–4787, https://doi.org/10.5194/amt-17-4777-2024, 2024.

Warwick, L., Oetjen, H., Murray, J., Panditharatne, S., Brindley, H., Schuettemeyer, D., Chen, X., and Huang, X.: In Situ Measurements of Ice and Snow Emissivity in the Far-Infrared, Earth and Space Science, 12, e2025EA004 350, https://doi.org/10.1029/2025EA004350, 2025.

Yang, P., Mlynczak, M. G., Wei, H., Kratz, D. P., Baum, B. A., Hu, Y. X., Wiscombe, W. J., Heidinger, A., and Mishchenko, M. I.: Spectral signature of ice clouds in the far-infrared region: Single-scattering calculations and radiative sensitivity study, Journal of Geophysical Research: Atmospheres, 108, https://doi.org/https://doi.org/10.1029/2002JD003291, _eprint: https://agupubs.onlinelibrary.wiley.com/doi/pdf/10.1029/2002JD003291, 2003.

Yu, Y. and Yu, P.: Land Surface Temperature Product from the GOES-R Series, in: The GOES-R Series, pp. 133–144, Elsevier, ISBN 978-0-12-814327-8, https://doi.org/10.1016/B978-0-12-814327-8.00012-3, 2020.